Action kinematics as an organising principle in the cortical control of human hand movement

James Kolasinski*, Diana C. Dima, David M. A. Mehler, Alice Stephenson, Sara Valadan, Slawomir Kusmia, Holly E. Rossiter

Cardiff University Brain Research Imaging Centre, School of Psychology, Cardiff University, Maindy Road, CF24 4HQ

Abstract

Hand movements are controlled by neuronal networks in primary motor cortex (M1)[1,2,3]. The organising principle encoding hand movements in M1 does not follow an anatomical body map, but rather a distributed representational structure in which motor primitives are combined to produce motor outputs[4,5]. Electrophysiological recordings in primates suggest that M1 neurons encode kinematic features of movements, such as joint position and velocity[6,7,8,9,10]. Human imaging data concur: relative differences in movement kinematics are mirrored by differences in the associated patterns of M1 activity[3,11]. However, M1 exhibits well-documented sensory responses to cutaneous and proprioceptive stimuli[12], raising questions regarding the origins of kinematic motor representations: are they relevant in top-down motor control, or are they an epiphenomenon of bottom-up sensory feedback during movement? Here we show that the kinematic signature of a wide variety of naturalistic hand movements is encoded in human M1 prior to the point of movement initiation. Using a powerful combination of high-field fMRI and MEG, a spatial and temporal multivariate representational similarity analysis revealed that patterns of M1 activity mirrored kinematic, but not muscle-based features of naturalistic hand movements prior to movement onset. Comparable M1 activity was not observed for an ethological action model based functional mappings proposed in M1[13]. Our spatial and temporal analyses provide firm evidence that the top-down control of dexterous movements activates cortical networks in M1 encoding hand kinematics.

1. Main text

Mounting evidence supports the encoding of movements in M1 based on kinematics and synergistic muscle activation, rather than the anatomy of

*Corresponding author
Email address: kolasinskij@cardiff.ac.uk (James Kolasinski)

the peripheral musculature[4,5]. Measurements from individual M1 neurons in non-human primates reveal the encoding of multiple kinematic features, such as speed, direction, and position in the same cells in a time-varying manner[6]. The same neuronal populations have been shown to encode instantaneous features during motor execution, as well as the target kinematic end point and upcoming movement trajectory[7,8,9,10].

In the human brain, evidence of neuronal tuning to multiple kinematic features has been reported during the production of intended movements from M1 microelectrode recordings made in tetraplegic patients[14]. The encoding of kinematic features of hand movements in M1 has also been supported by human imaging studies. Patterns of fMRI activity in sensorimotor cortex have been shown to mirror the relative differences in the final joint configuration across a range of prehensile movements[11]. Similarly, the representational structure of fMRI activity in M1 during finger flexion is consistent with patterns of finger co-use during naturalistic hand movements[3].

However, the functional relevance of kinematic encoding in M1 to human motor control remains a fundamental unknown. As well as their role in motor output, M1 neurons exhibit rapid and integrative responses to somatosensory signals[12,15]. Kinematic information is inextricably linked to proprioceptive and tactile signals: specific patterns of movement are associated with specific patterns of sensory feedback. Are kinematic motor representations reported in human M1 functionally relevant in the process of top-down motor control, or an epiphenomenon generated by bottom-up sensory feedback during human movement production?

We addressed this question using a spatiotemporal multivariate representational similarity analysis to ask where in the human brain and when during movement production are the kinematics of human hand movements encoded? This approach combined high-field fMRI and MEG data with kine-

Hand movements	
Abduct fingers	Pinch: thumb and little finger
Cylinder Grip	Pinch: thumb and index finger
Hook Grip	Pinch: thumb and middle finger
Spherical Grip	Pinch: thumb and ring finger
Index finger flexion (45°)	Ring finger flexion (45°)
Index finger flexion (90°)	Ring finger flexion (90°)
Index and middle finger flexion (90°)	Ring and little finger flexion (90°)
Index finger and thumb roll	Rock fingers
Little finger flexion (45°)	Squeeze: thumb and fingers
Little finger flexion (90°)	Abduct thumb
Middle finger flexion (45°)	Extend thumb
Middle finger flexion (90°)	Flex thumb
Middle and ring finger flexion (90°)	Twiddle: thumb and index finger

Table 1: Outline of the 26 hand movements used in the motor task. Instructional videos presented in Video S1.

matic data glove recordings made during a broad repertoire of prehensile and non-prehensile hand movements. Probing recordings of human brain activity with high spatial resolution from fMRI and high temporal resolution from MEG offers a powerful means to identify the location and timing of kinematic information encoding. Together this information was used to dissociate the relevance of kinematic information in M1 to top-down or bottom-up processes in motor control, as well as a relevance of alternative muscle-based or ethological action based models.

Ten right-handed participants performed a range of 26 prehensile and non-prehensile hand movements[16,17] (Table 1, Video S1) in two fMRI sessions (1.5 hours total fMRI data per participant), two MEG sessions (1.5 hours total MEG data per participant), and a behavioural testing session (35 minutes kinematic data recording). In each session participants wore a right-handed 14-channel fibre optic data glove; kinematic data were recorded throughout all sessions. Electromyography (EMG) data were acquired during MEG sessions to validate the movement onset measures calculated from the data

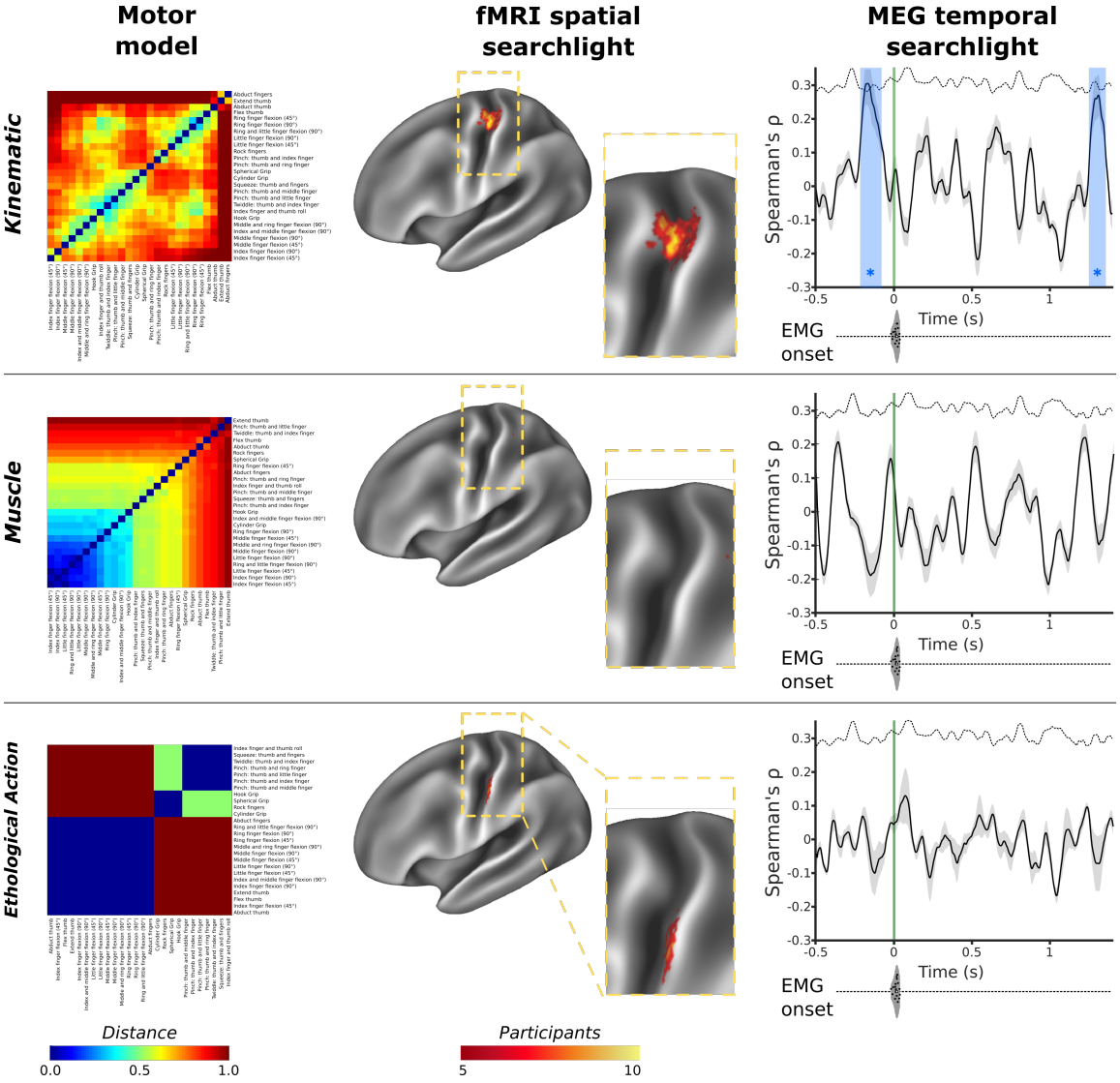

Figure 1: Spatial and temporal evidence for the encoding of hand kinematics in primary motor cortex prior to movement production. Kinematic, muscle, and ethological action models of hand movement were used in a spatiotemporal representational similarity analysis. Top row: fMRI data show that kinematic information was encoded consistently in primary motor cortex across all ten participants; complementary MEG data revealed temporal encoding of kinematic information (blue box) prior to movement onset (green line). The muscle model (middle row) and ethological action model (bottom row) showed very limited evidence of encoding, outside of M1 in the post-central gyrus and offered no evidence of significant temporal encoding during movement production. MEG temporal searchlight plots: data presented are from beta band analysis; full analysis presented in Figure 4, green line - movement onset defined by the data glove; blue regions - significant peaks in representational similarity between MEG data and the motor model; dashed line - correlation noise ceiling. EMG onset violin plots based on data presented in Figure S10. Model matrices reproduced in a larger format in Figure S2.

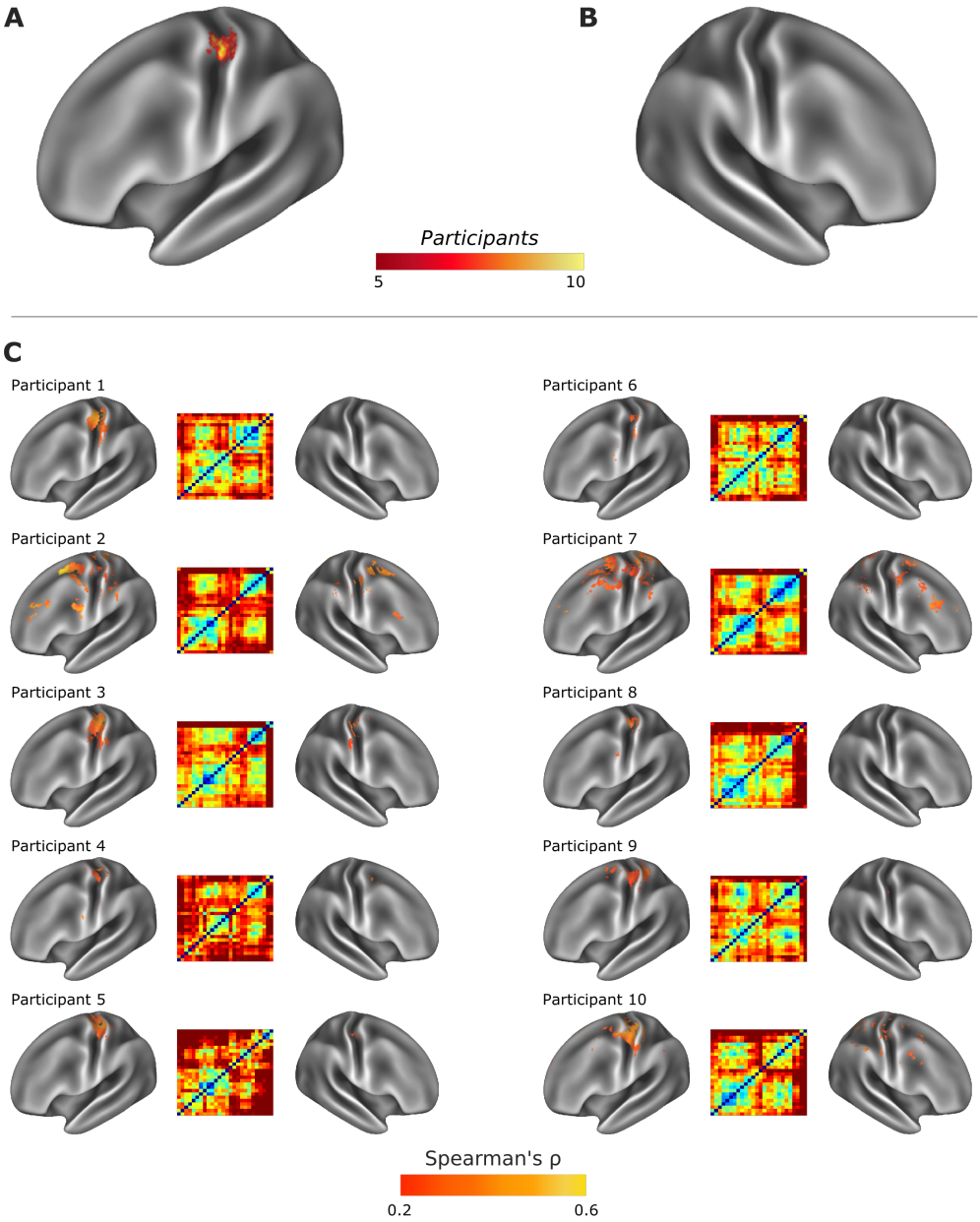

Figure 2: Single participant fMRI representational similarity analysis cortical searchlights using individual kinematic models of hand movement. Cortical heatmaps of the left (A) and right (B) hemisphere, show consistent encoding of kinematic information in the left motor cortex, contralateral to movement. Heatmaps were constructed from individually thresholded cortical searchlights for each participant, derived using their own kinematic model (C) (Omnibus threshold, $\alpha = 0.01$, maximum accuracy distribution calculated from peak correlation value across 10,000 searchlight permutations with label-switching). Supra-threshold range of Spearman's ρ for each participant presented in Table S2.

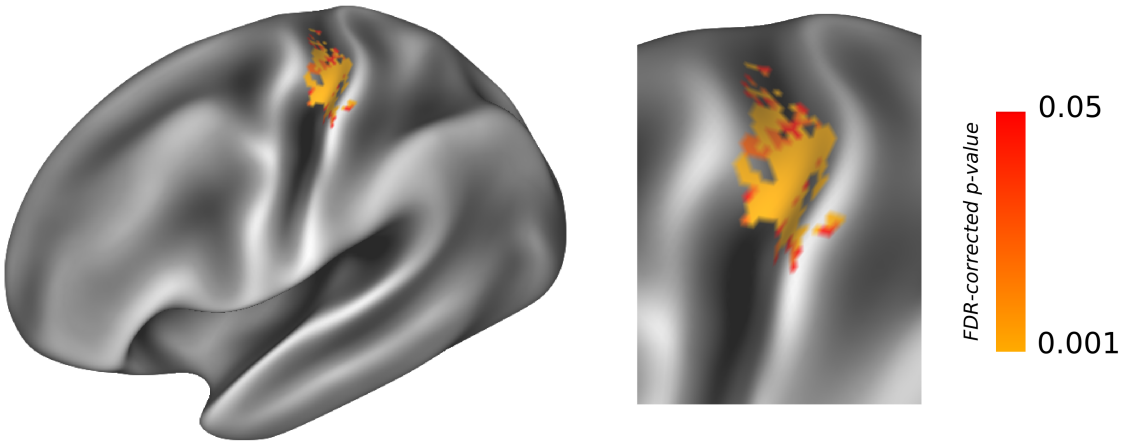

Figure 3: Comparison of movement models in spatial searchlight analysis reveals a significantly greater model fit for the kinematic model over the muscle model. Wilcoxon signed-rank test (one-sided) test applied to the difference between the kinematic and muscle model rho-value maps. Significant region of kinematic model fit aligned with Brodmann Area 4. Statistical maps subject to FDR correction ($\alpha = 0.05$).

glove.

To probe the spatial and temporal correspondence between patterns of brain activity and hand kinematics, data glove recordings were used to construct a kinematic model quantifying the similarity of the kinematic signals measured during each of the 26 movements (Figure 1: Top row, Figures S2 and S3). The kinematic model quantified the distance between the displacement measures for each movement pair across the 14 channels (Pearson correlation), subject to a Fisher Z-transformation and averaged across the 14 recording channels. The resulting kinematic model exhibits strong split-half and inter-session consistency within participant (Figure S1). A grand average of the kinematic model across sessions and participants was subject to non-classical multidimensional scaling for visualisation of the relative dissimilarity of each movement across two dimensions (Video S2). In both the spatial and temporal representational similarity analysis, the kinematic model was investigated

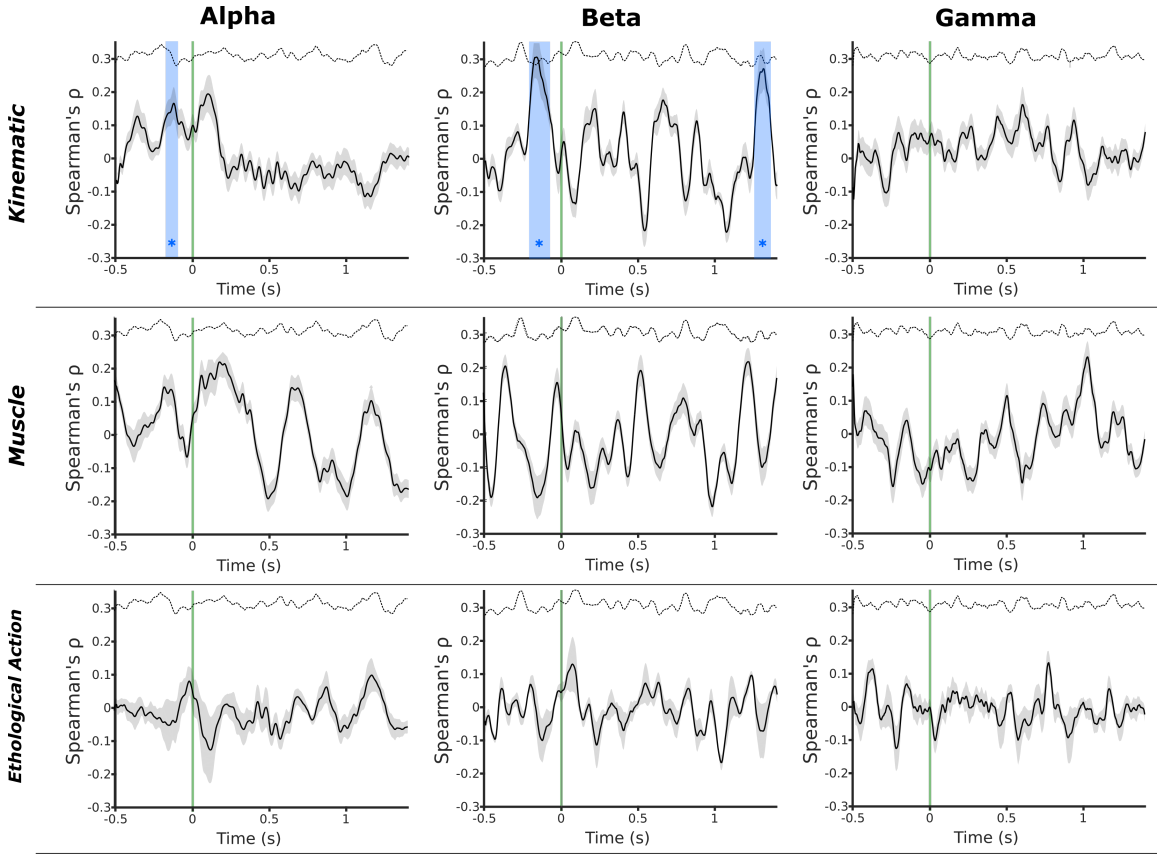

Figure 4: MEG temporal representational similarity analysis searchlight in motor cortex reveals encoding of kinematic information prior to movement onset. Temporal MEG searchlight analysis reveals evidence of the kinematic encoding of hand movements prior to movement onset (green bar). Distinct significant peaks in the correspondence between the kinematic model and MEG data (blue) were observed in the beta band (-210 ms to -85 ms) and the alpha band (-175 ms to -115 ms). An additional significant peak in the beta band analysis was observed after movement onset (1260 ms - 1350 ms). No such significant peaks were observed for the muscle model or ethological action model. Green line - movement onset defined by the data glove; blue regions - significant peaks in representational similarity between MEG data and the model; dashed line - correlation noise ceiling.

alongside two other models. A muscle based model was constructed from high-density EMG recordings (15 channels) made in an independent cohort of 10 participants performing the same range of hand movements (Figure 1: Middle row). An additional ethological action model classified movements into precision prehensile, power prehensile, and non-prehensile, based on the notion of ethological maps in primate M1[13] (Figure 1: Bottom row).

We first used high-resolution fMRI data to perform a cross-validated cortical surface-based searchlight representational similarity analysis to find evidence for the spatial encoding of kinematic information during movement. In each participant and each cortical searchlight, the unsmoothed pattern of fMRI activity during movement was used to construct a representational dissimilarity matrix (RDM)[18]. The RDM was compared to the participant's individual kinematic model, resulting in representational similarity surface maps of Spearman's ρ values for each participant, which were subject to an omnibus threshold ($\alpha = 0.01$; suprathreshold range for each participant outlined in table S2) and used to construct a cross-participant heatmap. This analysis assessed where the relative dissimilarities in the kinematic recordings across the different hand movements were mirrored by the relative differences in the pattern of fMRI activity elicited by performing the same movements. The searchlight revealed a strong and consistent representational similarity in the contralateral pre-central region of the anatomical hand-knob[19] across participants (Figure 1). Specifically, the fMRI searchlight results revealed the consistent encoding of the kinematic information in Brodmann Area 4 during the production of hand movements across participants (Table 2)[20].

Inspection of the single-subject cortical searchlight results for the kinematic model highlights the consistent and spatially limited correspondence of the kinematic model and fMRI data at the level of individual participants and

models in contralateral M1 (Figure 2A). A highly comparable result was also observed using the kinematic model constructed from the data glove recordings made in the behavioural testing session (Figure S4), highlighting the applicability of this result to real-world hand use in an upright sitting position. No such consistent representational similarity was observed in the corresponding searchlight of movement-related activity in the ipsilateral hemisphere at the group level (Figure 2B and Figure S4B).

Equivalent spatial searchlight analyses for the muscle model and the ethological action models revealed more limited evidence of consistent cortical encoding across participants, centred on somatosensory cortex in the post-central gyrus; specifically Brodmann Area 3b (Figure 1). Inspection of the single-subject cortical searchlights for both of the muscle and ethological action models again revealed more limited evidence of representational similarity in pre-central and parietal regions (Figures S6 and S7). In light of the interest in contrasting the kinematic and muscle models[11], a Wilcoxon signed-rank test (one-sided) was used to demonstrate the superior fit of the kinematic model in comparison to the muscle model in a localised region principally corresponding to Brodmann Area 4[18] (Figure 3).

Ultra high field fMRI data analysed at the level of individual subjects offered detailed spatial resolution, revealing the encoding of kinematic information in the hand knob region of M1. However, fMRI offers relatively poor temporal resolution to understand the point in time at which the kinematic model matches the pattern of brain activity. The boundary between motor and somatosensory cortex is increasingly blurred by evidence of sensory processing in M1[12] and motor modulation of sensory afferents[21]. The observed representational similarity of fMRI activity and hand kinematics may result from top-down control of motor function or bottom-up proprioceptive information passed back to M1 and S1. In order to dissociate the driving force

behind the kinematic model fit observed in the fMRI data, a temporal representational similarity analysis of MEG data was used to identify the point during movement preparation or execution at which kinematic information is encoded in the M1.

A cross-validated fixed-effects representational similarity analysis was applied, comparing a group average kinematic model derived from data glove recordings made in the MEG scanner to the pattern of alpha (7-14 Hz), beta (15-30 Hz), and gamma (30-100 Hz) band MEG brain activity in M1 (Figure S9) in 20 ms sliding windows during movement preparation and execution. The muscle model and ethological action model were assessed in equivalent analyses. In light of the interest in contrasting the kinematic and muscle models, the kinematic and muscle models were each assessed in a partial correlation to discount the contribution of the other.

In both the alpha and beta band analysis, there was significant correspondence between the MEG data and the kinematic model both preceding movement onset, and in the case of the beta band, after movement onset (Figure 4). In the beta band, the kinematic model mirrored the pattern of brain activity in a significant peak from -210 ms to -85 ms relative to movement onset (peak Spearman's ρ: 0.32). There was also a significant peak in the correspondence between the kinematic model and MEG data in the beta band after movement onset in the beta band (1260 - 1350 ms; peak Spearman's ρ: 0.35).

In the alpha band a correspondence between the kinematic model and MEG data was observed prior to movement onset from -175 ms to -115 ms (peak Spearman's ρ: 0.37). No significant peaks were observed in the correspondence between the M1 MEG signal in the alpha, beta, or gamma band and either the muscle model or the ethological action model (Figure 4).

Model	**Peak heatmap overlap (Participants)**	**Peak Vertex**	**Anatomical location**
Kinematic	10	8052	Area 4
Muscle	4	1904 4781 7266 11766	Area 2 VIP SCEF Area 23c
Ethological	8	8070	Area 3b

Table 2: Outline of peak anatomical correspondence between movement models and fMRI calculated using across participant cortical heatmaps. Peak regions calculated as centre of gravity of areas of peak overlap; peaks separated by a minimum of 20mm. Vertex positions and anatomical definitions are based on HCP S1200 32k release [20].

An analogous MEG temporal searchlight analysis during action observation revealed limited evidence of a correspondence between the kinematic model and brain activity in the alpha band in action observation during the movement videos preceding each movement block (Figure S5). During action observation a correspondence between the MEG signal and kinematic model was observed from 315 ms - 380 ms in the beta band, relative to stimulus onset (peak Spearman's ρ: 0.32). No peaks in any frequency band were observed for the muscle model or the ethological action model during the period of video observation.

Taken together, the MEG and fMRI results presented here strongly implicate the encoding of kinematic information in M1 as an organising feature in the top-down control of movement, rather than as a result of bottom-up sensory signals elicited by motor activity.

Using 7T fMRI we pinpointed a consistent encoding of kinematic information firmly in a localised region of Brodmann area 4 in M1. A temporal multivariate analysis of MEG data allowed us to further unpack this result, delving into the encoding of hand kinematics during the production of an individual movement. Using MEG, we observed that the encoding of this

kinematic information occurs prior to the onset of a movement. In other words, the relative differences in the kinematic structure of a range of different hand movements is encoded in M1 up to 210 ms before the onset of movement can be detected in the hand.

Information contained in the kinematic model showed temporally distinct correspondence to information contained in the alpha and beta bands of the MEG data. From 210 ms to 90 ms before movement is detected, the representational structure in the M1 beta band corresponds significantly to the representational similarity of the kinematics of the upcoming movement. The correspondence between the kinematic model and the information contained in the beta frequency band is consistent with the broad literature concerning the role of this oscillatory frequency in motor control. Beta oscillations are observed at rest; it is well established that beta activity is suppressed immediately prior to and during movement: movement-related beta desynchronisation (MRBD), and then rebounds following movement cessation: post-movement beta rebound (PMBR)[22]. The magnitude of the reduction in beta-band power observed prior to movement onset in motor cortex has been shown previously to relate to the degree of uncertainty in the upcoming movement[23] or action anticipation[24]. Previous comparisons of beta desychronisation made across kinematic and kinetic tasks concur: the strength of MRBD is correlated with the physical kinematic displacement of a given hand movement rather than the magnitude of muscle contraction[25]. Similar patterns of desynchronisation are observed in alpha band activity, where ERD in M1 corresponds to increased activation in the region[22], with post-motion event related synchronisation in M1[26]. Here we demonstrate that there is a link between information contained in the alpha and beta frequencies in M1 before movement onset and the subsequent kinematics of hand movements (Figures 1 and 4), suggesting that important information

about the upcoming motor command may be encoded within these oscillations[25,27]. A significant peak was also observed post-movement beta-band analysis; it be could be speculated that this peak represents information encoding of kinematic information around the time PMBR is known to occur after movement, or could reflect afferent inputs to M1[28]; these two possibilities cannnot be dissociated by the current experiment.

In contrast to alpha and beta frequencies, we observed no concurrence between the information contained in the gamma-frequency and the kinematic model. An increase in the amplitude of gamma oscillations has previously been reported during motor execution: movement-related gamma synchronisation (MRGS)[29,30]. In contrast to alpha and beta frequencies, evidence from studies of gamma oscillations report changes only after movement onset, and therefore would not be implicated in the encoding of information in M1 prior to movement, consistent with the data herein[31,32,33].

Hand kinematics have previously been investigated in the context of human fMRI. Relative differences in target joint position at the end of a hand movement have been shown previously to mirror the relative differences in the fMRI signal in a broad region sensorimotor cortex[11]. Additional work considering unidigit and multidigit flexion has demonstrated that patterns of M1 fMRI activity associated with such movements are better explained by kinematic models of digit co-use than by competing muscle-based models[3]. In the present study we have used MEG to fundamentally extend on these findings, demonstrating a top-down role for kinematic encoding prior to movement onset. Furthermore by using a kinematic model that compared the displacement trajectory of each movement rather than a single joint position, it was possible to contrast the kinematic features of both prehensile and non-prehensile movements to explore cortical encoding relevant to a full range of naturalistic hand use. Moreover, by capitalising on the gains in spa-

tial and temporal resolution afforded by using 7T fMRI and a limited field of view, we have been able to firmly pinpoint the spatial location at which kinematic information is encoded to the motor region of the anatomical hand knob, corresponding principally to Brodmann Area 4[19]. The fMRI spatial searchlight analysis did not reveal evidence of consistent encoding of kinematic information in ipsilateral M1 across participants (Figure 2). Previous fMRI studies provide evidence for the activation of ipsilateral M1 during the production of individual uni-digit movements[34,35] but not multi-digit sequences of uni-digit movements[36]. This study considered a broad array of naturalistic hand movements, engaging a wide variety of hand kinematics, involving simultaneous and/or sequential movement of different digits. It is possible that unlike sequences of uni-digit movement, these more complex movements do not drive the circuits of ipsilateral M1 as uni-digit movements do[34,35].

Previous studies have made direct comparisons between muscle-based models and kinematic models, arguing for the latter as an organising principle in the encoding of hand movements[3,11]. Here, a model constructed from an independently acquired set of high-density EMG recordings did not reveal any evidence for the spatial or temporal encoding of information on the basis of differences in muscle activity across the range of 26 hand movements under study. In addition, the kinematic model showed a superior representational similarity to the fMRI dataset than the muscle model in primary motor cortex (Figure 3). As with previous studies, these findings do not rule out the existence of muscle representations in M1, but rather support the existence of highly organised muscle representations structured around movement kinematics rather than anatomy. The assertion perhaps explains the fractures and repetitions observed in muscle representations during the search for an M1 body map[2].

The ethological action model also reported less consistent patterns of fMRI encoding, centred on the postcentral gyrus, consistent with activation in S1 (Figure 1). The ethological action model also did not reveal any significant peak in the temporal representational analysis. It is possible that while at a coarse level, ethological maps exist in the primate cortex, the concept of ethological organisation does not extend down to the fine-grain level of individual encoding of human hand movements; in other words, the broad motor reportoire of the human hand may not be encoded on the basis of the functional role of each movement. However, in the case of the primate, the coarser division of movements based on the functional role of the entire upper limb, including the hand (e.g. feeding, reaching), may play a role in the way the cortex is organised[37]. The observed patterns of post-central activity may alternatively result from selective disinhibition of S1 by M1 during motor activity, though such direct cortico-cortical signalling remains speculative in the human brain[21,38,39].

Analysis of the action observation period of the MEG data preceding each movement block also provided some support for the kinematic encoding of information in M1 (Figure S5). Previous MEG data acquired during action observation have demonstrated characteristic changes in M1 activity comparable to action execution[40]. Analyses of event related desynchronisation (ERD) in M1 during action observation suggest a peak change in the mu frequency as the observed movement evolves[41]. These observations are potentially consistent with the pattern of kinematic model fit observed in the beta band MEG data early during action observation (315 - 380 ms after stimulus onset), when the trajectory of movement has become clear (Figure S5). Additional work considering the encoding of kinematic information in oscillatory alpha band activity in M1 suggests that the observation of stimuli consistent with biological motion is sufficient to induce ERD in this

frequency band[42], potentially consistent with the notion that during observation of biological motion, M1 may encode kinematic information.

The data presented in this study rely on complementary information acquired from BOLD fMRI and MEG, though the remit of this work does not extend to fusion of the two modalities. BOLD fMRI provides only an indirect measure of neuronal activity based on haemodynamic changes associated with the execution of a given task[43], which can be resolved with a relatively high degree of spatial specificity with 7T imaging. In contrast, MEG reflects a more direct, temporally-rich, measure of neuronal activity. While the origins of the measured signals differ, compelling recent evidence provides non-coincidental data to support the notion of shared information across MEG and fMRI measures of brain activity across a wide range of frequency bands[44]; similar correspondences have been reported from invasive electrocorticography data[45]. However, the spatial component of MEG data must be inferred from mathematical modelling. Despite advances in the context of MEG source localisation, this feature of MEG analysis limits the spatial specificity of the measured signals, which integrate information across relatively large tissue volumes in comparison with fMRI[46]. We have harnessed the spatial and temporal strengths of fMRI and MEG, which in combination provide greater insight regarding the encoding of movements in M1 than the sum of their individual parts.

Here we apply a rich multi-modal design with multivariate analysis to demonstrate that the encoding of kinematic information in human M1 occurs prior to the onset of a wide range of naturalistic hand movements, in contrast to competing muscle and ethological action models. Mounting evidence for the encoding of complex kinematic information in M1 from this and other work continues to blur the boundary between primary somatosensory and primary motor cortex: even M1 neurons have been shown to rapidly con-

solidate sensory torque information across multiple joints[15]. The notion of kinematic representation in M1 is compatible with recent evidence of the tight integration of information across the central sulcus[47], whereby S1 encodes the current body state, while M1 encodes the kinematics necessary to achieve the intended body state. Such a system of motor control would see kinematic information encoded prior to movement onset as a prediction for the future sensory inputs expected by S1 when a movement has been achieved[48].

Acknowledgments

J.K. holds a Wellcome Trust Sir Henry Wellcome Postdoctoral Fellowship (204696/Z/16/Z). CUBRIC is supported by a Strategic Award from the Wellcome Trust (104943/Z/14/Z). This study was supported by the UK MEG Partnership Grant (MRC/EPSRC, MR/K005464/1). The authors are grateful to Krish Singh for his advice regarding the MEG analysis and for his comments on the manuscript, and to Yi-Jhong Han for his technical assistance with EMG data acquisition.

References

[1] W. Penfield, E. Boldrey, Somatic motor and sensory representation in the cerebral cortex of man as studied by electrical stimulation, Brain 60 (1937) 389–443.

[2] R. Lemon, The output map of the primate motor cortex, Trends in Neurosciences 11 (1988) 501–506.

[3] N. Ejaz, M. Hamada, J. Diedrichsen, Hand use predicts the structure of representations in sensorimotor cortex., Nat. Neurosci. 18 (2015) 1034–1040.

[4] S. A. Overduin, A. dAvella, J. M. Carmena, E. Bizzi, Microstimulation Activates a Handful of Muscle Synergies, Neuron 76 (2012) 1071–1077.

[5] S. A. Overduin, A. d'Avella, J. Roh, J. M. Carmena, E. Bizzi, Representation of Muscle Synergies in the Primate Brain, Journal of Neuroscience 35 (2015) 12615–12624.

[6] Q. G. Fu, D. Flament, J. D. Coltz, T. J. Ebner, Temporal encoding of movement kinematics in the discharge of primate primary motor and premotor neurons, Journal of Neurophysiology 73 (1995) 836–854.

[7] M. M. Churchland, K. V. Shenoy, Temporal complexity and heterogeneity of single-neuron activity in premotor and motor cortex, Journal of Neurophysiology 97 (2007) 4235–4257.

[8] N. G. Hatsopoulos, Q. Xu, Y. Amit, Encoding of movement fragments in the motor cortex, Journal of Neuroscience 27 (2007) 5105–5114.

[9] T. N. Aflalo, M. S. A. Graziano, Possible origins of the complex topographic organization of motor cortex: reduction of a multidimensional space onto a two-dimensional array., Journal of Neuroscience 26 (2006) 6288–6297.

[10] M. Saleh, K. Takahashi, N. G. Hatsopoulos, Encoding of coordinated reach and grasp trajectories in primary motor cortex, Journal of Neuroscience 32 (2012) 1220–1232.

[11] A. Leo, G. Handjaras, M. Bianchi, H. Marino, M. Gabiccini, A. Guidi, E. P. Scilingo, P. Pietrini, A. Bicchi, M. Santello, E. Ricciardi, A synergy-based hand control is encoded in human motor cortical areas, eLife 5 (2016) e13420.

[12] N. Hatsopoulos, A. Suminski, Sensing with the Motor Cortex, Neuron 72 (2011) 477–487.

[13] M. S. A. Graziano, Ethological Action Maps: A Paradigm Shift for the Motor Cortex, Trends in Cognitive Sciences 20 (2016) 121–132.

[14] W. Truccolo, G. M. Friehs, J. P. Donoghue, L. R. Hochberg, Primary Motor Cortex Tuning to Intended Movement Kinematics in Humans with Tetraplegia, Journal of Neuroscience 28 (2008) 1163–1178.

[15] J. A. Pruszynski, I. Kurtzer, J. Y. Nashed, M. Omrani, B. Brouwer, S. H. Scott, Primary motor cortex underlies multi-joint integration for fast feedback control, Nature 478 (2011) 387–390.

[16] Elliott J. M., Connolly K. J., A classification of manipulative hand movements, Developmental Medicine & Child Neurology 26 (1984) 283–296.

[17] L. A. Jones, S. J. Lederman, Human Hand Function, Oxford University Press, 2006.

[18] H. Nili, C. Wingfield, A. Walther, L. Su, W. Marslen-Wilson, N. Kriegeskorte, A toolbox for representational similarity analysis., PLoS Comput. Biol. 10 (2014) e1003553.

[19] T. A. Yousry, U. D. Schmid, H. Alkadhi, D. Schmidt, A. Peraud, A. Buettner, P. Winkler, Localization of the motor hand area to a knob on the precentral gyrus. A new landmark., Brain 120 (Pt 1) (1997) 141–157.

[20] M. F. Glasser, T. S. Coalson, E. C. Robinson, C. D. Hacker, J. Harwell, E. Yacoub, K. Ugurbil, J. Andersson, C. F. Beckmann, M. Jenkinson,

S. M. Smith, D. C. V. Essen, A multi-modal parcellation of human cerebral cortex, Nature 536 (2016) 171–178.

[21] S. Lee, G. E. Carvell, D. J. Simons, Motor modulation of afferent somatosensory circuits, Nat. Neurosci. 11 (2008) 1430–1438.

[22] G. Pfurtscheller, F. H. Lopes da Silva, Event-related EEG/MEG synchronization and desynchronization: basic principles, Clinical Neurophysiology 110 (1999) 1842–1857.

[23] C. Tzagarakis, N. F. Ince, A. C. Leuthold, G. Pellizzer, Beta-Band Activity during Motor Planning Reflects Response Uncertainty, Journal of Neuroscience 30 (2010) 11270–11277.

[24] D. Denis, R. Rowe, A. M. Williams, E. Milne, The role of cortical sensorimotor oscillations in action anticipation, NeuroImage 146 (2017) 1102–1114.

[25] K. Nakayashiki, M. Saeki, Y. Takata, Y. Hayashi, T. Kondo, Modulation of event-related desynchronization during kinematic and kinetic hand movements, Journal of NeuroEngineering and Rehabilitation 11 (2014) 90.

[26] S. Ohara, A. Ikeda, T. Kunieda, S. Yazawa, K. Baba, T. Nagamine, W. Taki, N. Hashimoto, T. Mihara, H. Shibasaki, Movement-related change of electrocorticographic activity in human supplementary motor area proper, Brain: A Journal of Neurology 123 (Pt 6) (2000) 1203–1215.

[27] A. K. Engel, P. Fries, Beta-band oscillationssignalling the status quo?, Current Opinion in Neurobiology 20 (2010) 156–165.

[28] H. Tan, C. Wade, P. Brown, Post-Movement Beta Activity in Sensorimotor Cortex Indexes Confidence in the Estimations from Internal Models, The Journal of Neuroscience: The Official Journal of the Society for Neuroscience 36 (2016) 1516–1528.

[29] D. Cheyne, S. Bells, P. Ferrari, W. Gaetz, A. C. Bostan, Self-paced movements induce high-frequency gamma oscillations in primary motor cortex, NeuroImage 42 (2008) 332–342.

[30] M. Nowak, C. Zich, C. J. Stagg, Motor Cortical Gamma Oscillations: What Have We Learnt and Where Are We Headed?, Current Behavioral Neuroscience Reports 5 (2018) 136–142.

[31] S. D. Muthukumaraswamy, Functional Properties of Human Primary Motor Cortex Gamma Oscillations, Journal of Neurophysiology 104 (2010) 2873–2885.

[32] D. Cheyne, P. Ferrari, MEG studies of motor cortex gamma oscillations: evidence for a gamma "fingerprint" in the brain?, Frontiers in Human Neuroscience 7 (2013) 575.

[33] K. J. Miller, G. Schalk, E. E. Fetz, M. den Nijs, J. G. Ojemann, R. P. N. Rao, Cortical activity during motor execution, motor imagery, and imagery-based online feedback, Proceedings of the National Academy of Sciences of the United States of America 107 (2010) 4430–4435.

[34] J. Diedrichsen, T. Wiestler, J. W. Krakauer, Two Distinct Ipsilateral Cortical Representations for Individuated Finger Movements, Cereb. Cortex 23 (2013) 1362–1377.

[35] E. Berlot, G. Prichard, J. O'Reilly, N. Ejaz, J. Diedrichsen, Ipsilateral finger representations are engaged in active movement, but not sensory processing, bioRxiv (2018) 285809.

[36] A. Yokoi, S. A. Arbuckle, J. Diedrichsen, The Role of Human Primary Motor Cortex in the Production of Skilled Finger Sequences, Journal of Neuroscience 38 (2018) 1430–1442.

[37] M. S. A. Graziano, C. S. R. Taylor, T. Moore, Complex movements evoked by microstimulation of precentral cortex, Neuron 34 (2002) 841–851.

[38] S. Lee, I. Kruglikov, Z. J. Huang, G. Fishell, B. Rudy, A disinhibitory circuit mediates motor integration in the somatosensory cortex., Nat. Neurosci. 16 (2013) 1662–1670.

[39] I. Choi, J.-Y. Lee, S.-H. Lee, Bottom-up and top-down modulation of multisensory integration, Current Opinion in Neurobiology 52 (2018) 115–122.

[40] R. Hari, N. Forss, S. Avikainen, E. Kirveskari, S. Salenius, G. Rizzolatti, Activation of human primary motor cortex during action observation: A neuromagnetic study, Proceedings of the National Academy of Sciences 95 (1998) 15061–15065.

[41] M. Tani, Y. Ono, M. Matsubara, S. Ohmatsu, Y. Yukawa, M. Kohno, T. Tominaga, Action observation facilitates motor cortical activity in patients with stroke and hemiplegia, Neuroscience Research 133 (2018) 7–14.

[42] Y. Meirovitch, H. Harris, E. Dayan, A. Arieli, T. Flash, Alpha and Beta Band Event-Related Desynchronization Reflects Kinematic Regularities, Journal of Neuroscience 35 (2015) 1627–1637.

[43] P. Jezzard, P. M. Matthews, S. M. Smith, Functional Magnetic Resonance Imaging, An Introduction to Methods, Oxford University Press, Oxford, 2001.

[44] J. F. Hipp, M. Siegel, BOLD fMRI Correlation Reflects Frequency-Specific Neuronal Correlation, Current biology: CB 25 (2015) 1368–1374.

[45] J. C. W. Siero, D. Hermes, H. Hoogduin, P. R. Luijten, N. F. Ramsey, N. Petridou, BOLD matches neuronal activity at the mm scale: a combined 7t fMRI and ECoG study in human sensorimotor cortex., NeuroImage 101 (2014) 177–184.

[46] E. L. Hall, S. E. Robson, P. G. Morris, M. J. Brookes, The relationship between MEG and fMRI, NeuroImage 102 Pt 1 (2014) 80–91.

[47] F. I. Arce-McShane, C. F. Ross, K. Takahashi, B. J. Sessle, N. G. Hatsopoulos, Primary motor and sensory cortical areas communicate via spatiotemporally coordinated networks at multiple frequencies, Proceedings of the National Academy of Sciences 113 (2016) 5083–5088.

[48] R. A. Adams, S. Shipp, K. J. Friston, Predictions not commands: active inference in the motor system., Brain Struct Funct 218 (2013) 611–643.

[49] R. C. Oldfield, The assessment and analysis of handedness: the Edinburgh inventory., Neuropsychologia 9 (1971) 97–113.

[50] J. Gross, S. Baillet, G. R. Barnes, R. N. Henson, A. Hillebrand, O. Jensen, K. Jerbi, V. Litvak, B. Maess, R. Oostenveld, L. Parkkonen, J. R. Taylor, V. van Wassenhove, M. Wibral, J.-M. Schoffelen, Good practice for conducting and reporting MEG research, Neuroimage 65 (2013) 349–363.

[51] J. W. Peirce, PsychoPy: Psychophysics software in Python, Journal of Neuroscience Methods 162 (2007) 8–13.

[52] J. W. Peirce, Generating stimuli for neuroscience using PsychoPy, Frontiers in Neuroinformatics 2 (2009).

[53] C. Blais, Random without replacement is not random: Caveat emptor, Behavior Research Methods 40 (2008) 961–968.

[54] E. Freud, S. N. Macdonald, J. Chen, D. J. Quinlan, M. A. Goodale, J. C. Culham, Getting a grip on reality: Grasping movements directed to real objects and images rely on dissociable neural representations, Cortex 98 (2018) 34–48.

[55] R. Oostenveld, P. Fries, E. Maris, J.-M. Schoffelen, FieldTrip: Open source software for advanced analysis of MEG, EEG, and invasive electrophysiological data, Computational Intelligence and Neuroscience 2011 (2011) 156869.

[56] Y. Zhang, M. Brady, S. Smith, Segmentation of brain MR images through a hidden Markov random field model and the expectation-maximization algorithm., IEEE Trans Med Imaging 20 (2001) 45–57.

[57] S. M. Smith, Fast robust automated brain extraction., Hum. Brain Mapp. 17 (2002) 143–155.

[58] M. Jenkinson, C. F. Beckmann, T. E. J. Behrens, M. W. Woolrich, S. M. Smith, FSL., NeuroImage 62 (2012) 782–790.

[59] A. M. Dale, B. Fischl, M. I. Sereno, Cortical surface-based analysis. I. Segmentation and surface reconstruction., NeuroImage 9 (1999) 179–194.

[60] B. Fischl, A. Liu, A. M. Dale, Automated manifold surgery: constructing geometrically accurate and topologically correct models of the human cerebral cortex., IEEE Trans Med Imaging 20 (2001) 70–80.

[61] M. Jenkinson, P. R. Bannister, M. Brady, S. Smith, Improved Optimization for the Robust and Accurate Linear Registration and Motion Correction of Brain Images, NeuroImage 17 (2002) 825–841.

[62] L. Griffanti, G. Douaud, J. Bijsterbosch, S. Evangelisti, F. Alfaro-Almagro, M. F. Glasser, E. P. Duff, S. Fitzgibbon, R. Westphal, D. Carone, C. F. Beckmann, S. M. Smith, Hand classification of fMRI ICA noise components, NeuroImage 154 (2017) 188–205.

[63] M. F. Glasser, S. N. Sotiropoulos, J. A. Wilson, T. S. Coalson, B. Fischl, J. L. Andersson, J. Xu, S. Jbabdi, M. Webster, J. R. Polimeni, D. C. Van Essen, M. Jenkinson, WU-Minn HCP Consortium, The minimal preprocessing pipelines for the Human Connectome Project, NeuroImage 80 (2013) 105–124.

[64] M. Jenkinson, S. Smith, A global optimisation method for robust affine registration of brain images., Med Image Anal 5 (2001) 143–156.

[65] D. N. Greve, B. Fischl, Accurate and robust brain image alignment using boundary-based registration, NeuroImage 48 (2009) 63–72.

[66] A. Walther, H. Nili, N. Ejaz, A. Alink, N. Kriegeskorte, J. Diedrichsen, Reliability of dissimilarity measures for multi-voxel pattern analysis, NeuroImage 137 (2016) 188–200.

[67] N. N. Oosterhof, T. Wiestler, P. E. Downing, J. Diedrichsen, A comparison of volume-based and surface-based multi-voxel pattern analysis, NeuroImage 56 (2011) 593–600.

[68] J. Diedrichsen, N. Kriegeskorte, Representational models: A common framework for understanding encoding, pattern-component, and representational-similarity analysis, PLoS Computational Biology 13 (2017).

[69] J.-D. Haynes, A Primer on Pattern-Based Approaches to fMRI: Principles, Pitfalls, and Perspectives, Neuron 87 (2015) 257–270.

[70] J. D. Power, K. A. Barnes, A. Z. Snyder, B. L. Schlaggar, S. E. Petersen, Spurious but systematic correlations in functional connectivity MRI networks arise from subject motion, NeuroImage 59 (2012) 2142–2154.

[71] J. Vrba, S. E. Robinson, Signal Processing in Magnetoencephalography, Methods 25 (2001) 249–271.

[72] G. Nolte, The magnetic lead field theorem in the quasi-static approximation and its use for magnetoencephalography forward calculation in realistic volume conductors, Physics in Medicine and Biology 48 (2003) 3637–3652.

[73] B. D. V. Veen, W. V. Drongelen, M. Yuchtman, A. Suzuki, Localization of brain electrical activity via linearly constrained minimum variance spatial filtering, IEEE Trans. Biomed. Eng (1997) 867–880.

[74] M. Guggenmos, P. Sterzer, R. M. Cichy, Multivariate pattern analysis for MEG: A comparison of dissimilarity measures, NeuroImage 173 (2018) 434–447.

[75] O. Ledoit, M. Wolf, A well-conditioned estimator for large-dimensional covariance matrices, Journal of Multivariate Analysis 88 (2004) 365–411.

[76] N. Tzourio-Mazoyer, B. Landeau, D. Papathanassiou, F. Crivello, O. Etard, N. Delcroix, B. Mazoyer, M. Joliot, Automated anatomical labeling of activations in SPM using a macroscopic anatomical parcellation of the MNI MRI single-subject brain, NeuroImage 15 (2002) 273–289.

[77] T. E. Nichols, A. P. Holmes, Nonparametric permutation tests for functional neuroimaging: a primer with examples., Hum. Brain Mapp. 15 (2002) 1–25.

[78] J. D. Power, A. Mitra, T. O. Laumann, A. Z. Snyder, B. L. Schlaggar, S. E. Petersen, Methods to detect, characterize, and remove motion artifact in resting state fMRI, NeuroImage 84 (2014).

[79] S. Afyouni, T. E. Nichols, Insight and inference for DVARS, NeuroImage 172 (2018) 291–312.

2. Materials and Methods

2.1. Participants and Experimental Design

All data were acquired according to the local university research ethics committee approval in line with the Declaration of Helsinki (Cardiff University School of Psychology Research Ethics Committee: EC.17.03.14.4874 and EC.17.04.11.4885) All participants provided written informed consent and met local MRI and MEG safety criteria.

Ten right-handed participants were recruited in the main study (Age range: 22-30; Mean age: 24.0; Age SD: 2.8; 5 Female). Participants were not currently taking any psychoactive medications, and were right-handed according to the Edinburgh Handedness Inventory[49]. No participants had a history of any disorder affecting tactile sensory or motor function or any history of neurological illness. Each participant undertook five experimental sessions: two MRI scan sessions, two MEG recording sessions, and one behavioural testing session. All participants undertook the behavioural testing session first; the subsequent order of the fMRI and MEG sessions was counterbalanced, leaving a minimum of two weeks between any one MRI and MEG session to minimise the effects of magnetic noise on the MEG signal[50]. The datasets generated and analysed during the current study are available from the corresponding author on reasonable request.

2.2. Motor task and kinematic data acquisition

During all sessions participants were engaged in a motor task involving the production of a range of 26 hand movements (Table 1) with the right hand while wearing a fibre-optic kinematic data glove (Data Glove 14 Ultra; Fifth Dimension Technologies: 5DT, Orlando, FL, USA). Kinematic data were

acquired across 14 independent fibre optic channels (one proximal and one distal sensor per digit, plus one sensor between each digit pair) at 60 Hz. The behavioural task was implemented in PsychoPy (Version 1.84.20)[51,52] using the Python Computer Graphics Kit (CGkit: cgkit.sourceforge.net) SDK wrapper for the 5DT data glove.

Each recording session was divided into task runs; each task run was composed of blocks of a specific movement; each block comprised individual movement trials; details of the number runs, blocks, and trials are specified for MEG and fMRI sessions respectively below. Instructions were presented on a screen in the testing environment. Each task run contained one block of each of the 26 movement types, ordered using a random-without-replacement selection method. Progressive determination effects were minimised by maximising the range of different conditions in each run; presenting all 26 movements once per run[53]. At the beginning of each movement block, participants were shown a 3 second video of the movement to be produced (Video S1). Participants were cued to produce the movement in question in each subsequent movement trial of the block by an expanding and contracting horizontal bar. In each movement trial the bar began at a fully contracted width, coloured red, indicating that the hand should be static and in a resting flat position. The bar subsequently turned green and began to expand symmetrically at its left and right flanks. Once it reached its maximal width, the bar began to contract back to its original width. Once the bar reached its original contracted width, it turned red, signifying the end of the movement trial. Participants were instructed to pace their movements to coincide with the period of expansion and contraction of the green bar, such that their hand assumed a flat position at the beginning and end of each trial, corresponding to the time that the static red bar was presented. The motor task was conducted in a behavioural testing lab, in

the MRI scanner, and in the MEG scanner, as detailed below.

None of the grasping tasks in this study engaged participants with real objects; previous work has differentiated motor activity with or without real objects in anterior intraparietal sulcus, but not primary motor cortex: as such an object-free study design seemed appropriate for a study focusing on M1[54].

2.3. Kinematic recording session

During the behavioural testing session participants performed five runs of the motor task. Participants were seated at a desk with their right forearm supported on a memory foam mount, while wearing the data glove. Participants viewed instructions presented on a 14 inch laptop display. Each movement block comprised a 3 second video of the movement to be produced, a 1 second preparation period and 8 subsequent movement trials; each comprising 1.6 seconds of movement (green expanding/contracting bar), followed by a 0.8 second rest period (red static bar). The transition of the bar from red to green was defined as the go signal. A break period of up to 15 seconds was permitted between each movement block; participants advanced the task with a key-press using their left hand. Excluding break periods each task run was 10 minutes and 3.2 seconds in duration. The four task runs yielded 33 minutes and 16.8 seconds of kinematic data recording per participant.

2.4. Kinematic movement model

For each participant kinematic data from the behavioural, MRI, and MEG sessions were each processed in parallel. This yielded a separate kinematic model from each session type for each participant. These models were used

in subsequent multivariate fMRI and MEG analysis; they captured the kinematic similarities and differences of the 26 distinct movements under study.

Initially the kinematic data from each session and each movement block were epoched into individual movement trials using the time of onset of the green bars and averaged. The resulting 14 channels of data represented the average pattern of displacement of the hand during a movement trial for a given movement, termed the kinematics of the movement: the motion of the hand without reference to the forces that produce this motion. In order to compare this signature of kinematic activity for each possible pairing of the 26 movements the activity pattern of each of the 14 recording channels was correlated using Pearson's correlation coefficient, subject to the Fisher Z-transformation, and averaged to yield a single measure of the similarity of kinematics across each movement pair. The resulting value was transformed back into a Pearson's r-value and used to construct a 1-r dissimilarity matrix for each movement pair.

The kinematic dissimilarity matrices were averaged across task runs within-participant to yield an fMRI, MEG, and behavioural kinematic model for each participant. The split-half consistency and inter-session consistency of these models is outlined in Figure S1. A grand average across participant and session kinematic model (Figures 1 and S2) was computed and subject to hierarchical clustering; this resulting clustering was applied to all visualisations of the kinematic model.

2.5. Muscle model

An independent EMG dataset was acquired in order to construct a model of hand movement dissimilarity on the basis of muscle activity in the hand. An independent cohort of ten participants (Age range: 20-30; mean age:

25.1; age SD: 3.57; 5 female) undertook a more detailed EMG recording than was feasible during the MEG session, while performing the same 26 hand movement. EMG data were acquired using a Biosemi Active 2 system with a 32 channel headbox (Biosemi B.V. Amsterdam). Muscle activity was recorded using touchproof flat active electrodes. Electrodes 1-15 were placed as labelled in Figure S16, electrode 16 was used to rereference the EMG data in subsequent analysis and was placed on the bony protrusion of the elbow. There were also CMS and DRL electrodes, which served as a ground/reference during recording in the Biosemi software; they were placed on the palmar side of the wrist. The EMG data were recorded at 2048Hz.

The EMG recording sessions mirrored the design and setup of the kinematic recording session outlined above and were informed by previous fMRI MVPA studies of digit flexion[3]. Five runs were recorded in total, each containing 26 trials (one for each of the movements). The EMG data were processed using Fieldtrip[55]. EMG data were rereferenced to electrode 16, rectified and low-pass filtered (fourth order Butterworth filter: 40 Hz), and epoched relative to earliest measured muscle onset in any EMG channel using an adaptive threshold (activity duration threshold: 200ms) (Hooman Sedghamiz: Matlab File Exchange: Automatic Activity Detection in Noisy Signals using Hilbert Transform.) This results in individual trials of 2.0s in duration. These trials were baselined using the fixation cross window at the start of each trial. EMG trial data were then subject to multivariate noise normalisation by weighting channels in trial by the error covariance across the different channels in order to more accurate quantify the true differences between the muscle activity across different movements. The normalised trials were averaged into 5 folds. A Mahalanobis distance comparing each of the muscle activity of each of 26 different movement types was calculated using a cross-validated leave-one-out approach. In each iteration, the muscle

activity patterns from one fold were assigned to fold A and the muscle activity data from the remaining four folds were assigned to fold B; distances were calculated between all possible pairs of the 26 movement muscle activity recordings across these two folds (Equation (3)). Distance measures were calculated across all possible pairs of cross-validation folds. An average muscle model across all ten participants' data was generated and used to probe the spatial and temporal encoding of muscle based dissimilarities in the brain using fMRI and MEG (Figures 1 and S2).

2.6. Ethological action movement model

An alternative ethological action based model was constructed based on more recent evidence of ethological maps in primate M1[13], and therefore categorises movements on the basis of their specific action, namely prehensile movements, sub-categorised into precision grip and power grip, and non-prehensile movements[17] (Figure 1). The ethological action model was subject to hierarchical clustering for visualisation.

2.7. MRI data acquisition

MR data were acquired using a Siemens 7T Magnetom system (Siemens Healthcare, Erlangen, Germany) with a 32-channel head coil. Blood oxygenation level dependent (BOLD) fMRI was acquired with a T2*-weighted multi-slice gradient echo planar imaging (EPI). True axial slices were positioned for optimal coverage of the left and right anatomical hand knob[19] (TR/TE: 1500/25 ms, resolution: 1.2 mm isotropic, 22 axial slices, flip angle:90; GRAPPA factor: 2; anterior-posterior phase-encoding direction; 391 measurements). Magnetization prepared rapid gradient echo (MPRAGE) structural MRI data were acquired to facilitate BOLD EPI slice placement

and for cortical surface reconstruction (TR/TE: 2200/2.82 ms, isotropic resolution: 1.0 mm, GRAPPA factor = 2). An additional gradient echo BOLD EPI acquisition of 4 volumes was acquired using posterior-anterior phase-encoding direction for distortion correction.

2.8. fMRI behavioural task

During the fMRI acquisitions participants performed a total of ten runs of the motor task (5 runs per MRI session). Participants were led supine with their right forearm supported against their right hip and their elbow supported by a foam pad, while wearing the data glove. Participants viewed instructions via a mirror mounted on the transmit coil and a projector screen mounted at the end of the bore. Each movement block comprised of a 3 second instruction screen ("Prepare to Move"), a 3 second video of the movement to be produced, and a 1 second further instruction screen ("Move"), followed by 5 movement trials, each comprising 1.6 seconds of movement (green expanding/contracting bar), followed by a 0.4 second rest period (red static bar). Each movement block was 17 seconds. In addition to the movement blocks, 8 rest blocks were included in each task run; rest blocks were of equivalent duration to movement blocks and comprised of a 3 second instruction screen ("Rest"), a 3 second video of a static resting hand, and a 1 second further instruction screen ("Rest"), followed by the same period of expanding and contracting bar visual stimuli as the fMRI movement blocks. Rest blocks were positioned randomly in each run, excluding self-adjacency.

2.9. Structural MRI data preprocessing

MPRAGE data were subject to reorientation, bias-field correction and brain extraction using the FMRIB Software Library (FSL) fsl_anat tool[56,57,58] prior to cortical surface reconstruction using FreeSurfer Version 5.3.0[59,60].

2.10. fMRI data analysis

2.10.1. fMRI preprocessing and general linear modelling

fMRI data were subject to standard preprocessing, including motion correction with MCFLIRT[61], brain extraction using BET[57], and high pass temporal filtering (100 second threshold). fMRI data were not subject to spatial smoothing. All fMRI data were subject to manual independent components analysis denoising[62]. Distortion correction was undertaken using FSL Topup to estimate a fieldmap image for use in FSL FUGUE[63]. Undistorted BOLD EPI data were co-registered with structural MPRAGE data using Boundary-Based-Registration from FMRIB's Linear Registration Tool (FLIRT) implemented in epi_reg[64,61,65]. Example fMRI timeseries from a single voxel located in the anatomical hand knob is presented for four participants on a single session in Figure S15.

For each participant and each fMRI run, fMRI data were analysed using a first-level general linear modelling (GLM) approach implemented in FSL FEAT[58] using FMRIBs Improved Linear Model (FILM) to estimate time series autocorrelation and pre-whiten each voxel. Each of the 26 movements was modelled with a separate boxcar regressor with gamma-HRF convolution and its temporal derivative, giving a total of 52 regressors. Parameter estimates were calculated, contrasting each movement type against the rest condition; these voxel-wise maps and an estimate of the residuals from the GLM were resampled into the respective participants' structural space and used in subsequent representational similarity analysis (RSA).

2.10.2. fMRI multivariate noise normalisation

In order to account for the spatial structure of the noise inherent to fMRI data, spatial prewhitening of the parameter estimates from each participant

and each fMRI task run was conducted. The residuals (R) from the first-level GLM analysis provided an estimate of data not fit by the model regressors across voxels (V) and time (T), from which a V x V covariance matrix ($\widehat{\Sigma}$) can estimate the noise structure across voxels (Equation (1))[66].

$$\widehat{\Sigma} = \frac{1}{T}\mathbf{R^T R} \tag{1}$$

The noise covariance structure was combined with the voxel-wise parameter estimates (P) for a given movement type (k) to generate a spatially pre-whitened parameter estimate (P_k^*: Equation (2)):

$$P_k^* = P_k \widehat{\Sigma}^{-\frac{1}{2}} \tag{2}$$

2.10.3. fMRI surface-based searchlight representational similarity analysis

A surface-based representational similarity analysis searchlight approach was used to identify regions in which the multivariate pattern of BOLD activity mirrored the kinematic and categorical models. This surface-based analysis constrained the voxels under consideration in each searchlight to the grey matter and prevented the issue of sampling of voxels that span a sulcus in a single searchlight, which is inherent to volumetric approaches[67]. A searchlight was constructed at the centre of each vertex within the individual participants' anatomical cortical surface region corresponding to the field of view of their task fMRI data (Figure S8). Each searchlight had a diameter of 10mm. The region of interest of each searchlight was projected from 2D surface to 3D volumetric space using the Connectome Workbench Tool[63], masked by a FMRIB Automatic Segmentation Tool grey matter map[56] and a mask excluding voxels spanning across sulci in the FreeSurfer reconstruction

to improve spatial specificity. Spatially pre-whitened parameter estimates were extracted from the resulting volumetric region corresponding to each searchlight.

2.10.4. fMRI cross-validated distance measures

Within each searchlight the similarity between each of the spatially pre-whitened voxel-wise parameter estimates corresponding to each of the 26 different movement types was calculated using a cross-validated leave-one-out approach to avoid the possibility of over-fitting the data[68,69]. In each iteration, the parameter estimate maps from one fMRI task run was assigned to fold A and the parameter estimate maps from the remaining nine task fMRI runs were assigned to fold B; squared Euclidean distances were calculated between all possible pairs of the 26 movement parameter estimate maps across these two folds (Equation (3)). Distance measures were calculated across all possible pairs of cross-validation folds and averaged[66]. The use of spatially pre-whitened parameter estimate combined with the cross-validation approach yielded cross-validated Mahalanobis distance representational dissimilarity matrices (RDMs) comparing each of the activation patterns across all possible pairings of the 26 movements. For example, calculation of the distance between movement k and movement l in one iteration:

$$d^2_{Crossvalidated\,Mahalanobis}\left(P^*_k, P^*_l\right) = \left(P^*_k - P^*_l\right)_A \left(P^*_k - P^*_l\right)^T_B \qquad (3)$$

The correspondence between the fMRI-derived RDM in each searchlight and the candidate kinematic and theoretical models was assessed using a Spearman's rank correlation, with the resulting ρ (rho) value was plotted in each searchlight's central vertex on the cortical surface. For statistical

inference a fixed effects randomisation test[18] was applied on the individual participant level: correlations using 10,000 condition-label randomisations were undertaken in each searchlight. From each of the permutations, the spatial peak ρ value (rho) was extracted from across the cortical surface, forming a maximum accuracy distribution from which an omnibus threshold ($\alpha = 0.01$) was extracted. The resulting thresholded ρ-value surface maps for each participant were resampled onto the Human Connectome Project 32k surface (S1200.L.pial.MSMAll.32k_fs_LR.surf.gii), binarised and used to form a heatmap corresponding to the spatial distribution of the each model fit across participants. In light of the interest in contrasting the kinematic and muscle models, a comparison of the corresponding unthresholded Spearman's ρ cortical surface maps was undertaken using a Wilcoxon signed-rank test (one-sided), subject to FDR correction ($\alpha = 0.05$).

2.11. fMRI motion considerations

Variability in the magnitude of fMRI motion across different movement conditions has the potential to influence the observed pattern of results. The potential for noise induced by participant motion has been mitigated in a number of ways. First, all data has been subject to ICA denoising to remove any characteristic motion artefacts[62]. Second, the multivariate analysis of fMRI data emoloyed herein used spatial prewhitening of the parameter estimates to account for voxel-wise variability in noise to not downweight voxels with high error variance and to account for noise covariance between voxels[66]. Finally DVAR values were calculated for each fMRI timeseries (D: temporal derivative of time courses, VARS: root mean squares variance over voxels). These values quantify for each frame of an fMRI acquisition the magnitude of signal intensity change in comparison in volume N compared with volume N-1, as per the following formula:

$$DVARS(\Delta I)_i = \sqrt{\left\langle [I_i(\overrightarrow{x}) - I_{i-1}\overrightarrow{x}]^2 \right\rangle} \quad (4)$$

Where I_i is image intensity at locus $\overrightarrow{x}$ on frame i; angle brackets denote the spatial average over the whole brain[70]. DVARs are able to quantify corruption of fMRI acqusition due to head motion. DVAR values were extracted for volumes corresponding to each of the 26 hand movements for all participants; the resulting distribution of DVAR values is presented in Figure S13. The profiles of very limited motion across participants during each session of around 10 minutes in duration also demonstrate high quality data acquisition (Figure S14).

2.12. MEG data acquisition

MEG signals were measured continuously at 1200Hz during the motor task using a whole-head 275-channel axial gradiometer CTF MEG system (CTF, Vancouver, Canada) located inside a magnetically shielded room. An additional 29 reference channels were recorded for noise cancellation purposes and the primary sensors were analysed as synthetic third-order gradiometers[71]. Three electromagnetic coils were placed on three fiduciary locations (nasion, left and right pre-auricular) and their position relative to the MEG sensors were recorded continuously during each experimental block. The head surface and fiducial locations were digitized using an ANT Xensor digitizer (ANT Neuro, Enschede, Netherlands) prior to the MEG recording.

2.13. MEG behavioural task

During the MEG data acquisitions participants performed a total of ten runs of the motor task (5 runs per MEG session). Participants were sitting upright with their right forearm and elbow supported on a foam armrest, while

wearing the data glove. Participants viewed instruction on a back-projected screen in front of them from a projector mounted outside the shielded room. Each movement block comprised of a 2 second period with a central fixation cross, a 3 second video of the movement to be produced, and a 1 second instruction screen ("Prepare to Move") followed by five movement trials, each comprising 1.6 seconds of movement (green expanding/contracting bar), followed by a 0.8 second rest period (red static bar). Each movement block was 18 seconds. The order of movement blocks was randomised within each task run; each movement was presented once per task run.

2.14. Data glove movement onset detection: MEG sessions

The 14 channels of data glove recordings collected during the MEG sessions were aligned with the MEG acquisitions using the onset of the green bar and were epoched alongside the MEG data. Epoched data glove recordings were subject to onset segmentation using an adaptive threshold (activity duration threshold: 200ms) (Hooman Sedghamiz: Matlab File Exchange: Automatic Activity Detection in Noisy Signals using Hilbert Transform.). A conservative estimate of movement onset was derived by taking the earliest signal onset detected across the fourteen data glove channels for each movement trial. The resulting movement onset time was used to epoch MEG data in further analysis.

2.15. MEG data analysis

2.15.1. MEG preprocessing

Each participant's head shape was digitized using Xensor digitizer software (ANT software BV, Enschede, The Netherlands). All MEG analysis was conducted using the Fieldtrip toolbox for EEG/MEG-analysis[55]

(Donders Institute for Brain, Cognition and Behaviour, Radboud University Nijmegen, the Netherlands. See http://www.ru.nl/neuroimaging/fieldtrip). Co-registration was performed in a two stage process: first the fiducial locations were marked on the T1 structural for that participant; the head digitization data was then used to align the data with the MRI, subject to manual adjustment. Alignment was undertaken independently for data from the two MEG sessions.

Data from each movement type were epoched from the 10 task runs and concatenated into a new dataset containing 10 blocks, each containing 5 movement trials. The fixation cross and movement trials were epoched from the overall block. The movement trials were defined relative to the data glove defined movement onset time (movement trial time: 2 s; pre-onset time: 0.5s, post-onset time: 1.5s). The fixation cross period was used as a baseline for the 5 movement trials within each movement block. A high pass filter of 1 Hz and a low pass filter of 100 Hz were applied. MEG analyses were conducted across three frequency bands: alpha (7-14 Hz), beta (15-30 Hz) and gamma (30-100 Hz). All of the movements trials for a given movement type were concatenated across the 10 task runs, creating a dataset comprising 50 repeats of a movement. At this point the data was visually inspected and those trials containing artefacts were removed from further analysis up to a maximum of 10 trials, such that the minimum number of movements trials per movement included in further analysis was 40.

2.15.2. MEG source reconstruction

In order to reconstruct oscillatory activity at brain locations directly comparable across participants, the individual anatomical MRI was non-linearly warped to the MNI MRI template. The MNI template was divided into a

10 mm isotropic grid and the inverse of the previously calculated non-linear warp was used to warp the template grid into the anatomical space of each participant. Sensor leadfields were calculated using a semi-realistic volume conduction model based on the individual anatomy[72]. The temporal evolution of source activation at each location in the brain was estimated using a linearly constrained minimum variance (LCMV) beamformer algorithm[73] with the optimal dipole orientation at each voxel estimated using singular value decomposition (SVD). Virtual sensors were then reconstructed from all 3294 voxels by multiplying the sensor level data by the corresponding set of optimised weights. At this stage data were subject to multivariate noise normalization[74,75]: we calculated the error covariance matrix at sensor level and then used this combined with the filters from the LCMV to create the virtual sensor data. This means that sensors with more noise would be down-weighted compared to those with less noise. At this stage the data was also down-sampled to 600 Hz to reduce computational cost.

2.15.3. MEG temporal representational similarity analysis

The MEG data were split to produce 10 partitions and then averaged within each partition to perform a cross-validated representational similarity analysis to avoid the possibility of over-fitting the data[68,69]. RSA was performed across time using a sliding time window with a width of 20 ms and a time step of 5 ms creating 396 time windows across 2 seconds of the movement trial (0.5s rest; 1.5s movement). After selecting virtual sensors within the left hemisphere motor region of the AAL atlas[76] (Precentral L, 31 sources; Figure S9), the frequency-filtered MEG signal measured during each movement type was compared using a cross-validated leave-one-out approach within each time width. In each iteration, the signals from one MEG data partition were assigned to fold A, and the signals from the remaining nine

partitions were assigned to fold B; squared Euclidean distances were calculated between all possible pairs of the 26 signals across the two folds and averaged[66]. The use of multivariate noise normalisation to account for spatial autocorrelation in the MEG signal yielded subject-wise cross-validated Mahalanobis distance RDMs comparing the alpha, beta, or gamma-band signal in the motor ROI across all possible pairings of the 26 movements[74].

Participant-level motor ROI RDMs were averaged in order to perform a fixed-effects analysis. The correspondence between the MEG-derived RDMs and the candidate kinematic and theoretical models across time was assessed using a Spearman's rank correlation, with the resulting ρ (rho) values plotted for each time window. In light of the interest in contrasting the kinematic and muscle models, these were each assessed in a partial correlation to discount the contribution of the other. Randomization testing was used for statistical inference[77], whereby candidate model RDMs were shuffled 1000 times and time-resolved correlation coefficients were recomputed in order to estimate an empirical null distribution. P-values were calculated using a cluster thresholding approach across time. To correct for multiple comparisons, the cluster-forming threshold was set to $P < 0.01$ and clusters in the correlation time-courses corresponding to each candidate model were thresholded against the maximal cluster distribution ($\alpha = 0.001$).

To assess the maximal correlation possible with our data, each participant's RDM was correlated with the average cross-subject RDM; the correlations were then averaged to obtain an upper bound of the noise ceiling[18].

2.15.4. MEG: action observation analysis

MEG from the period of action observation during the instruction video preceding each movement block were epoched using the same approach as

the MEG data recorded during movement. The fixation cross and action observation trials were epoched from the overall block. The action observation trial was defined relative to the video stimulus onset time (pre-onset time: 0.5s, post-onset time: 3.0s). The fixation cross period was used as a baseline for the action observation period. Temporal representational similarity analyses were conducted using the same apporoach as the MEG movement data, as described above.

2.15.5. MEG motion considerations

MEG analysis included multivariate noise normalisation to account partially for the effects of motion, where each channels are normalised by an estimate of error covariance across different sensors; this process has been demonstrated to substantially improve multivariate analyses of MEG data[74]. Motion parameters for all MEG acquisitions were extracted and analysed to rule out the possibility of excessive head motion as a potential driving force behind any observed patterns of brain activity. Rotational and translational displacement for each participant and each experimental session are presented in Figure S11. In addition, the motion parameters during each movement block were extracted and the resulting distribution is presented across the 26 different movement types (Figure S12). The profiles of motion across participants demonstrate a high quality data acquisition.

2.16. Electromyography with MEG

Electromyography (EMG) data were acquired simultaneously with MEG data. Three surface EMG electrodes were attached to the right hand underneath the data glove, positioned on abductor pollicis brevis (APB), first

dorsal interosseus (FDI) and abductor digiti minimi (ADM). The area under the electrodes was exfoliated and cleaned with alcohol prior to data acquisition. EMG signals were recorded at 1200Hz.

EMG data were initially subject to a bandpass filter (20-500Hz) and a notch filter (50 Hz). EMG data were epoched and baselined alongside the MEG data. Epoched EMG data were subject to manual artefact rejection. Signals from the three electrodes during each epoch were independently subject to a Hilbert transform and smoothing (5 ms window) prior to activity onset segmentation using an adaptive threshold (activity duration threshold: 200ms) (Hooman Sedghamiz: Matlab File Exchange: Automatic Activity Detection in Noisy Signals using Hilbert Transform.). A conservative estimate of muscle activity onset was derived by taking the earliest signal onset detected across the three EMG channels for each movement trial. Due to constraints of electrode placement alongside the kinematic data glove, measures of activity onset were not robustly measured in all participants. EMG onset data are presented in order to validate the data glove measures of movement onset, which have been used to epoch the MEG data (Figures 1 and S10).

Video S1: Compilation of instructional videos used at the beginning of movement blocks in all testing sessions. Movement labels are provided for reference only; labels were not included during the task (VideoS1.mov).

Video S2: Visualisation of multidimensional scaling of grand average kinematic model constructed across participants and sessions. (VideoS2.mov).

	Average	**St. Dev.**
Kinematic model: fMRI	0.6318 (0.6010-0.6627)	0.1027 (0.0850 - 0.1297)
Kinematic model: behavioural	0.5812 (0.5506-0.6119)	0.1021 (0.0845 - 0.1289)
Kinematic model: MEG	0.6577 (0.6328 -0.6826)	0.0828 (0.0686 - 0.1046)
Muscle model	0.5286 (0.4822-0.5749)	0.1542 (0.1276-0.1948)

Table S1: Inter-subject consistency of kinematic and muscle models. Spearman's ρ (rho) vales. Figures in brackets represent confidence intervals.

.

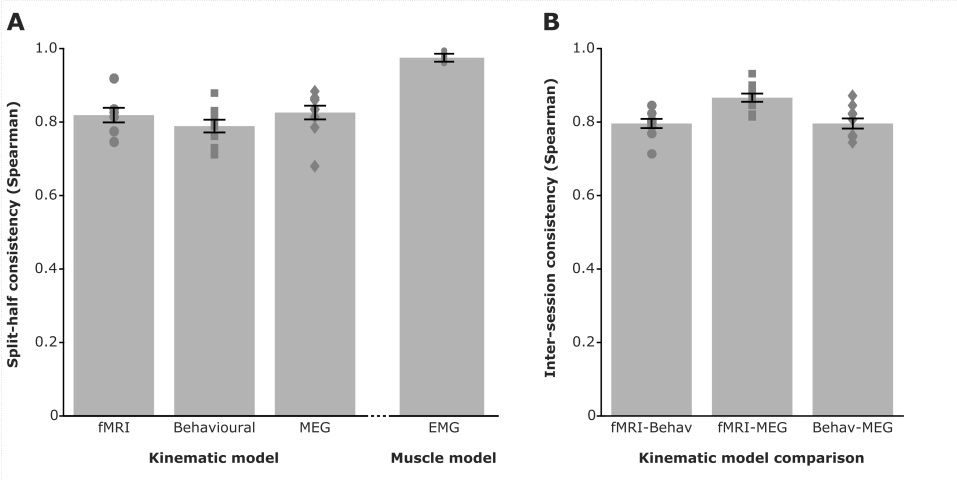

Figure S1: Data-driven kinematic models constructed for each participant and each session type exhibit strong split-half and inter-session consistency. Muscle model reproducibility data also presented.

	Kinematic (fMRI)		***Kinematic (Behav)***		***Ethological Action***		***Muscle***	
Participant	*Left-contra*	*Right-ipsi*	*Left-contra*	*Right-ipsi*	*Left-contra*	*Right-ipsi*	*Left-contra*	*Right-ipsi*
1	0.265 - 0.474	-	0.262 - 0.382	-	0.259 - 0.410	0.272 - 0.305	0.283 - 0.420	0.286 - 0.467
2	0.250 - 0.563	0.251 - 0.500	0.249 - 0.384	0.255 - 0.326	0.249 - 0.470	0.250 - 0.441	0.276 - 0.525	0.277 - 0.379
3	0.247 - 0.430	0.252 - 0.405	0.252 - 0.382	0.263 - 0.308	0.249 - 0.301	0.249 - 0.296	0.279 - 0.543	0.285 - 0.432
4	0.256 - 0.411	0.257 - 0.407	0.252 - 0.334	0.277 - 0.327	0.264 - 0.483	-	0.304 - 0.418	0.276 - 0.374
5	0.254 - 0.453	0.251 - 0.272	0.252 - 0.378	0.246 - 0.363	0.248 - 0.349	-	0.270 - 0.542	0.281 - 0.402
6	0.258 - 0.412	0.274 - 0.369	0.260 - 0.344	0.266 - 0.327	0.257 - 0.421	0.274 - 0.281	0.285 - 0.383	0.300 - 0.377
7	0.250 - 0.478	0.251 - 0.435	0.241 - 0.548	0.240 - 0.509	-	-	0.271 - 0.577	0.275 - 0.440
8	0.269 - 0.416	0.263 - 0.333	0.255 - 0.453	0.279 - 0.345	0.252 - 0.291	-	0.284 - 0.397	0.289 - 0.440
9	0.250 - 0.386	0.251 - 0.284	0.243 - 0.360	-	0.253 - 0.450	0.296 - 0.305	0.270 - 0.515	0.275 - 0.406
10	0.259 - 0.525	0.254 - 0.479	0.261 - 0.549	0.263 - 0.451	0.249 - 0.481	-	0.276 - 0.0.587	0.274 - 0.402

Table S2: Summary of supra-threshold Spearman's ρ (rho) values for each participant across each cortical surface searchlight. Data presented for left and right hemisphere. Kinematic behavioural session data were used to construct an additional model based on movement data outside of the scanner also used in an equivalent searchlight analysis to the fMRI kinematic model. Individual participant surfaces searchlights are presented in Figures 2, S4, S6 and S7).

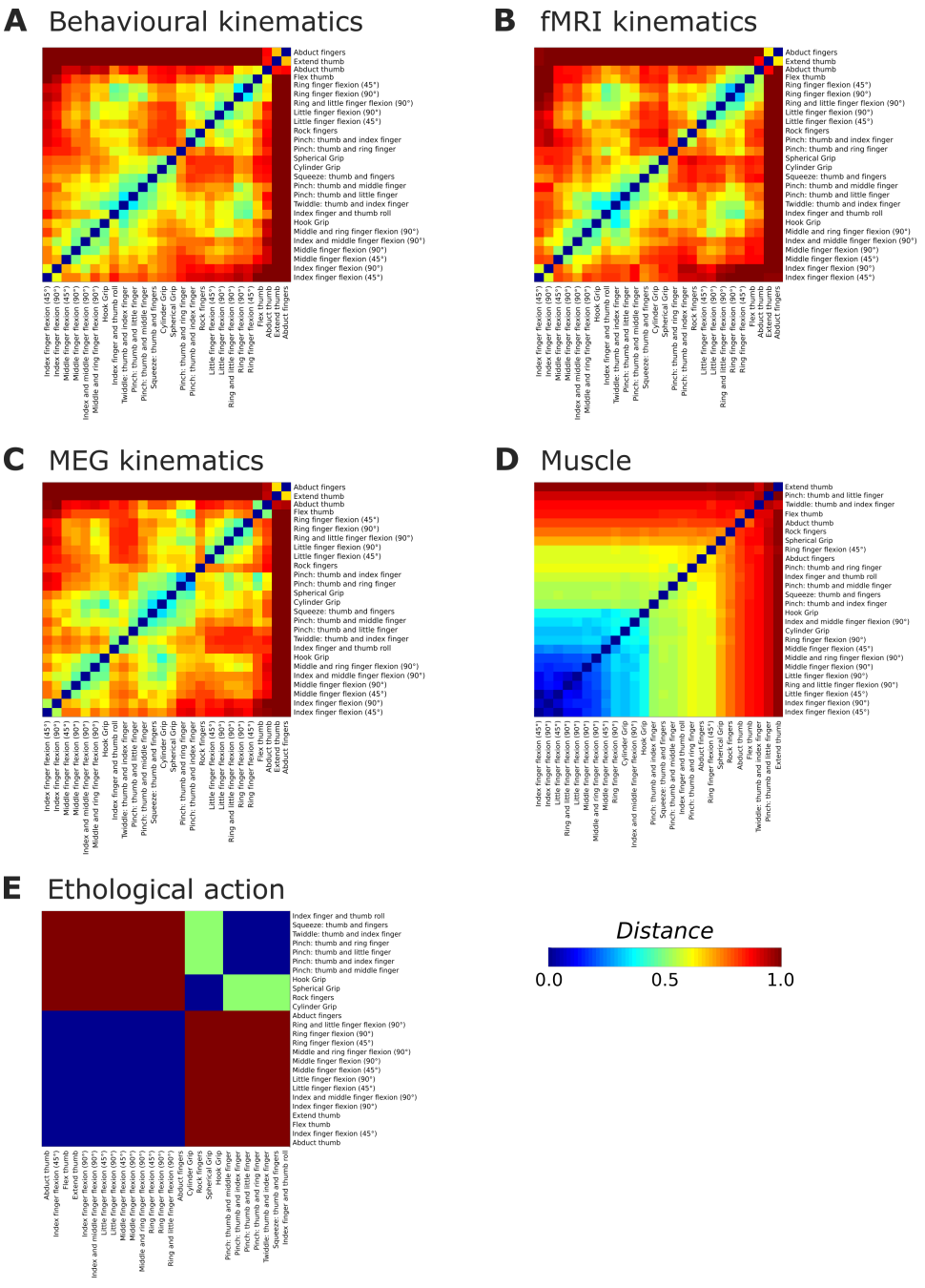

Figure S2: The average kinematic model across participants for each session type, the muscle model derived from an independent cohort of participants, and the categorical ethological action model.

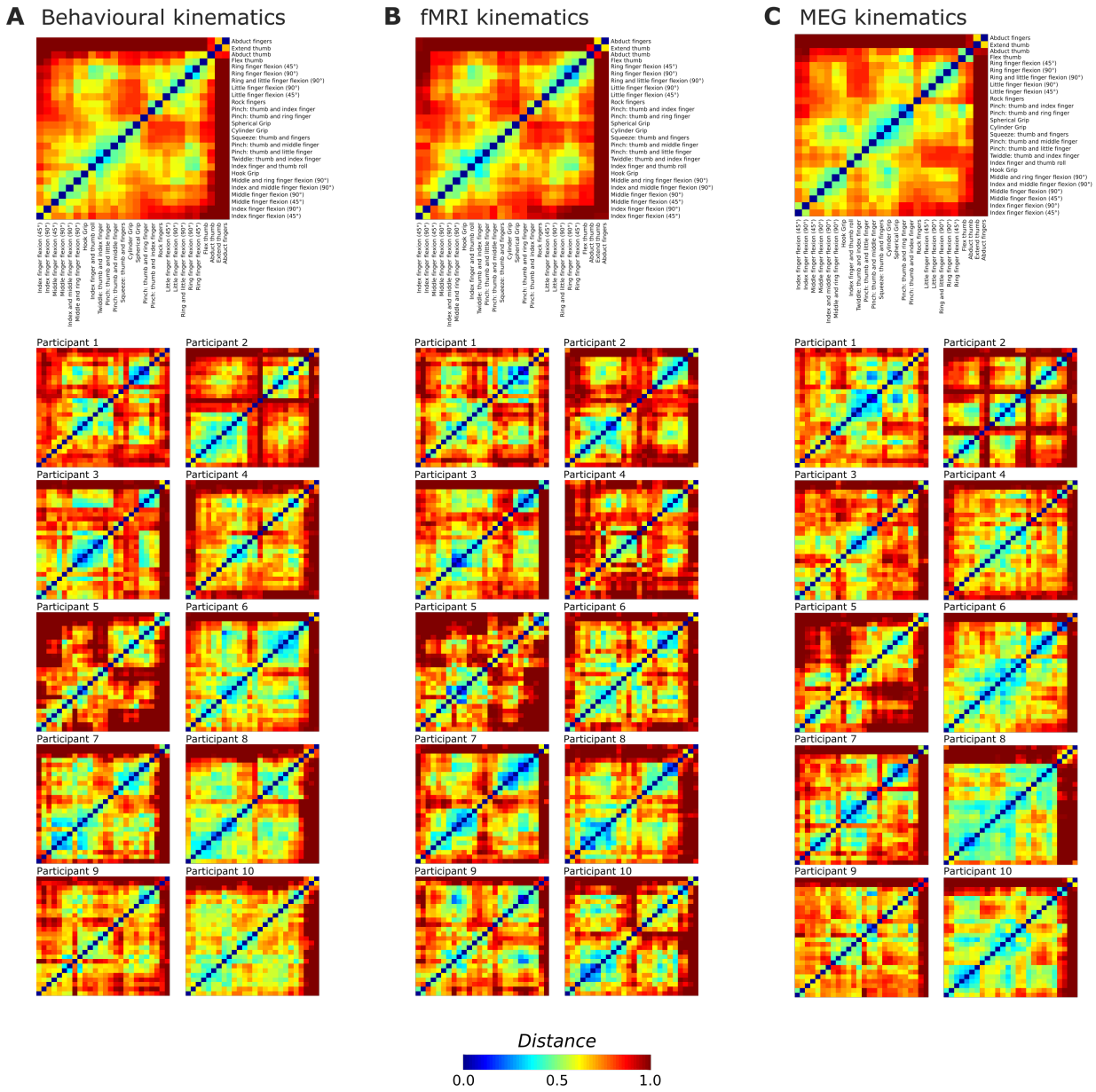

Figure S3: The average kinematic model constructed from the data glove measures acquired during the (A) behavioural session, (B) fMRI sessions, and (C) MEG sessions; presented alongside the individual subject models for each participant and session.

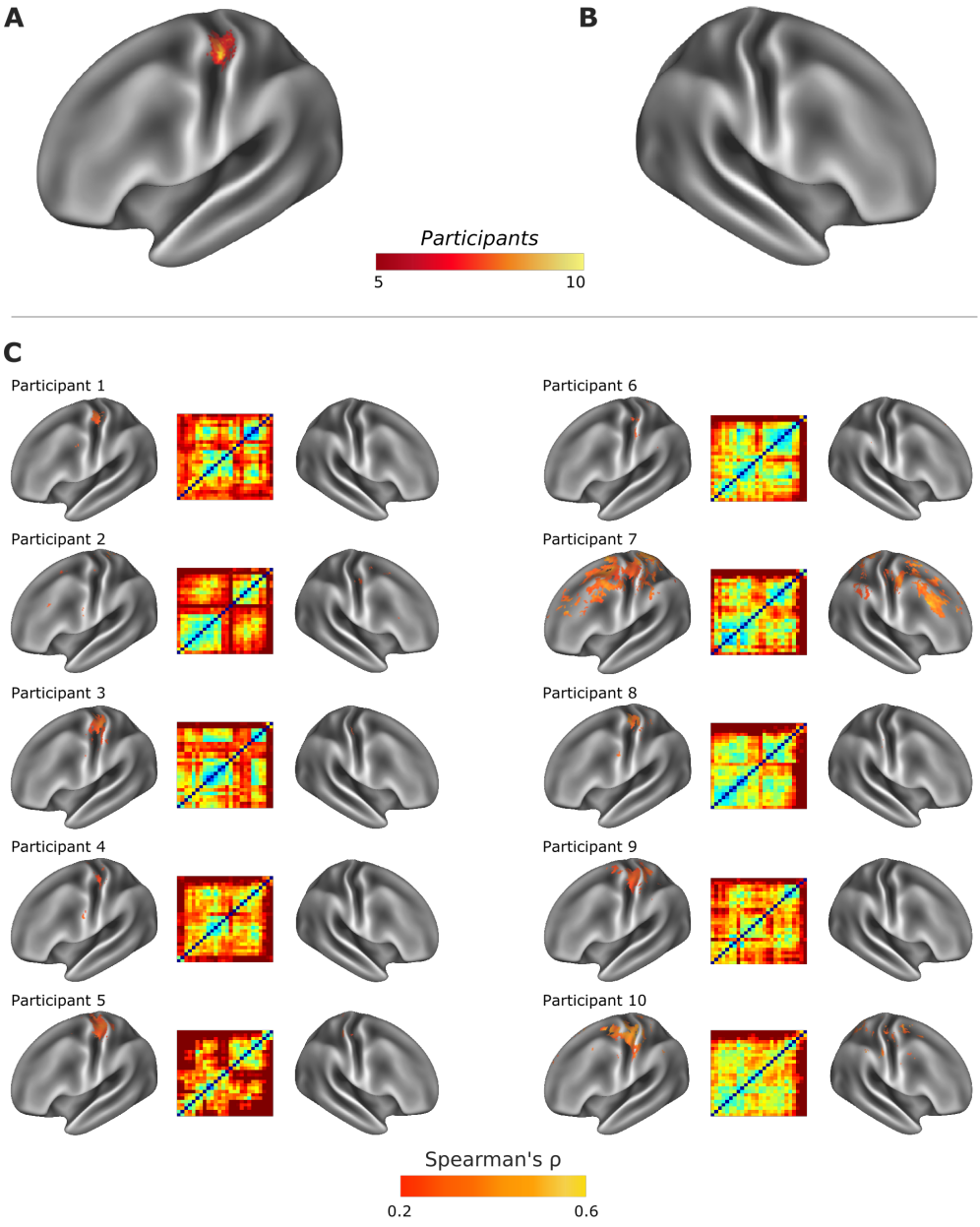

Figure S4: fMRI searchlight analysis conducted using the kinematic model constructed from data glove recordings made during the behavioural testing session. Evidence of the encoding of kinematic data in contralateral primary motor cortex persists using independent data glove recordings while participants were sitting upright in a more naturalistic position. Comparison with data presented in Figures 1 and 2. Supra-threshold range of Spearman's ρ for each participant presented in Table S2.

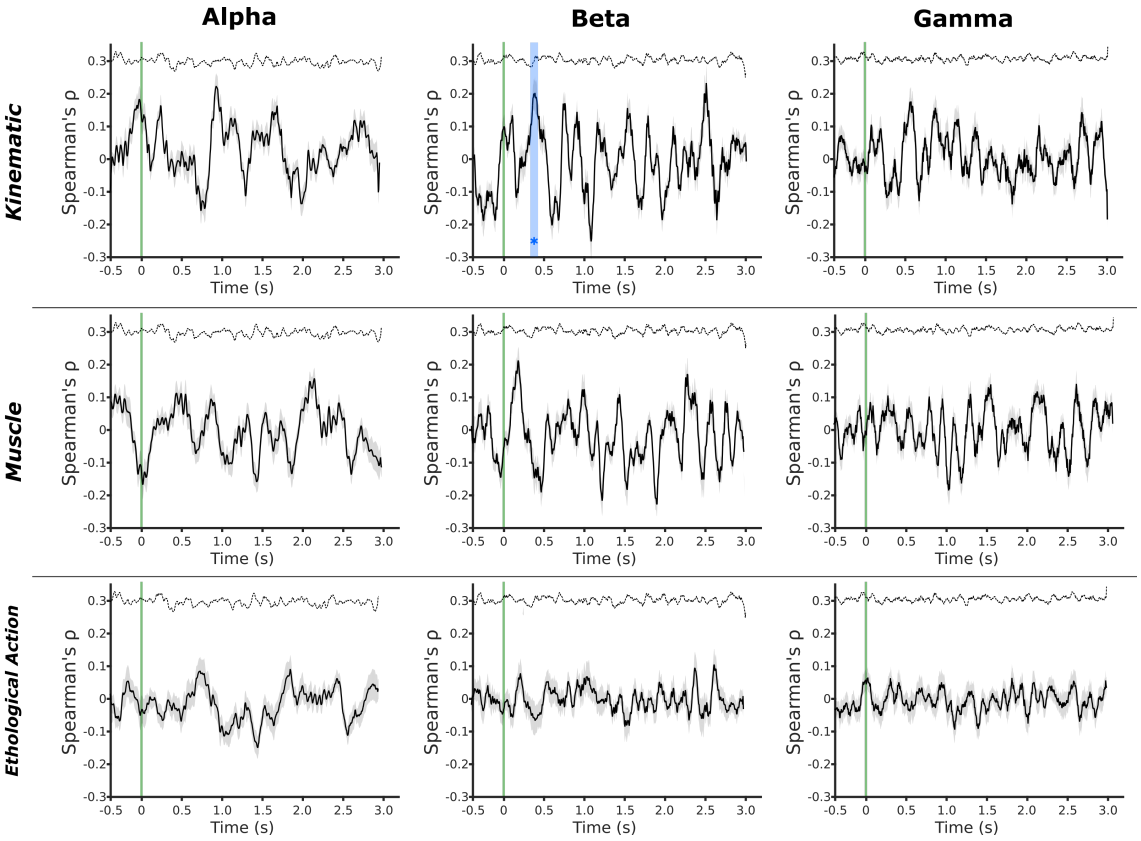

Figure S5: MEG searchlight analysis during action observation Evidence of a significant peak in the correspondence between the kinematic model and beta band MEG data in the period of action observation (315 ms - 380 ms). The green line indicates the onset of the stimulus video; the blue regions indicate significant peaks in representational similarity between MEG data and the motor model; the dashed line indicates noise ceiling. Comparison with MEG temporal searchlight results presented in Figures 1 and 4.

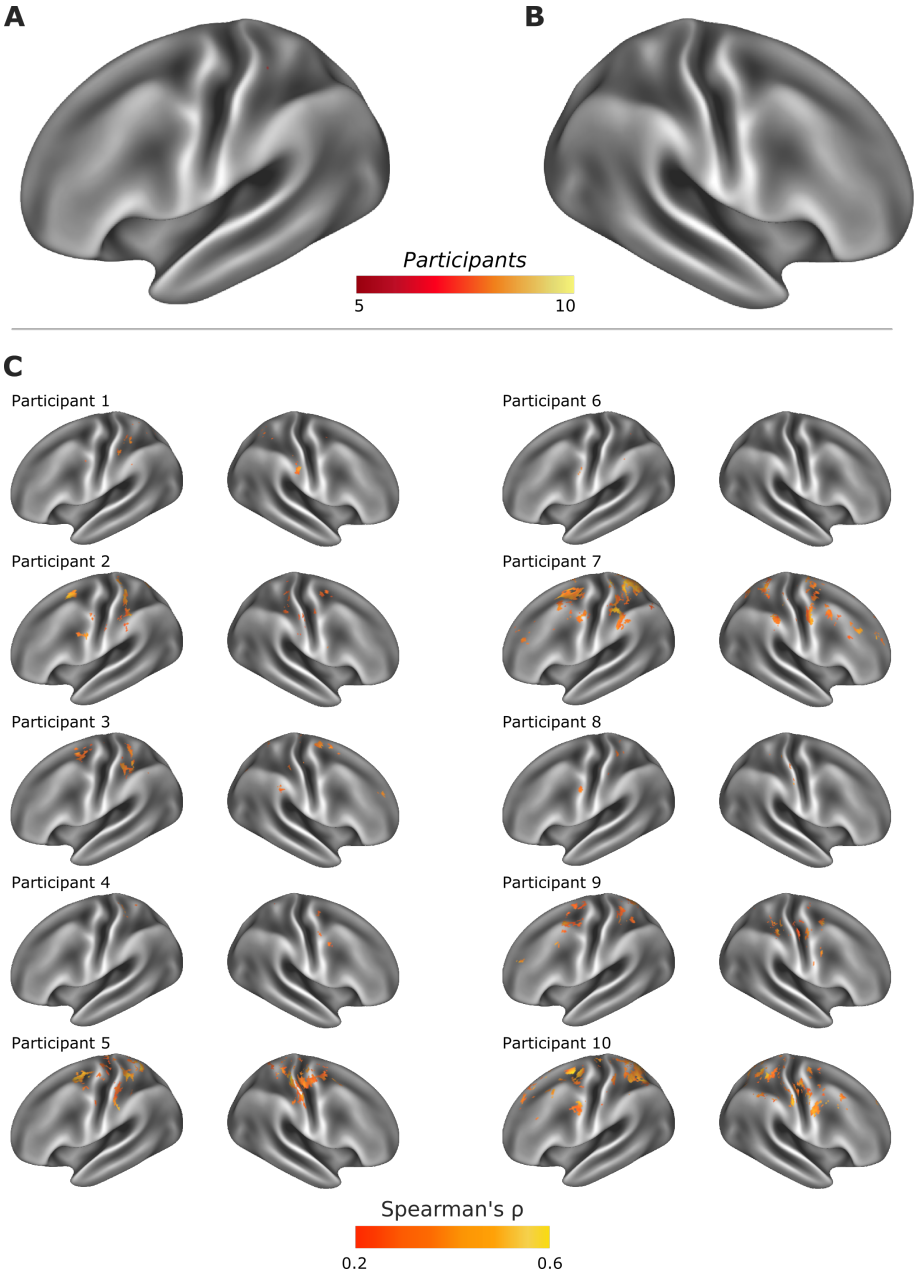

Figure S6: Individual participant cortical searchlight results using an muscle model of movement encoding. Cortical heatmaps of the left (A) and right (B) hemisphere, show limited but consistent encoding of an action model in the left post-central gyrus, contralateral to movement. Heatmaps were constructed from individually thresholded cortical searchlights for each participant using a single categorical action model (C) (Omnibus threshold, $\alpha = 0.01$, maximum accuracy distribution calculated from peak correlation value across 10,000 searchlight permutations with label-switching.) Supra-threshold range of Spearman's ρ for each participant presented in Table S2.

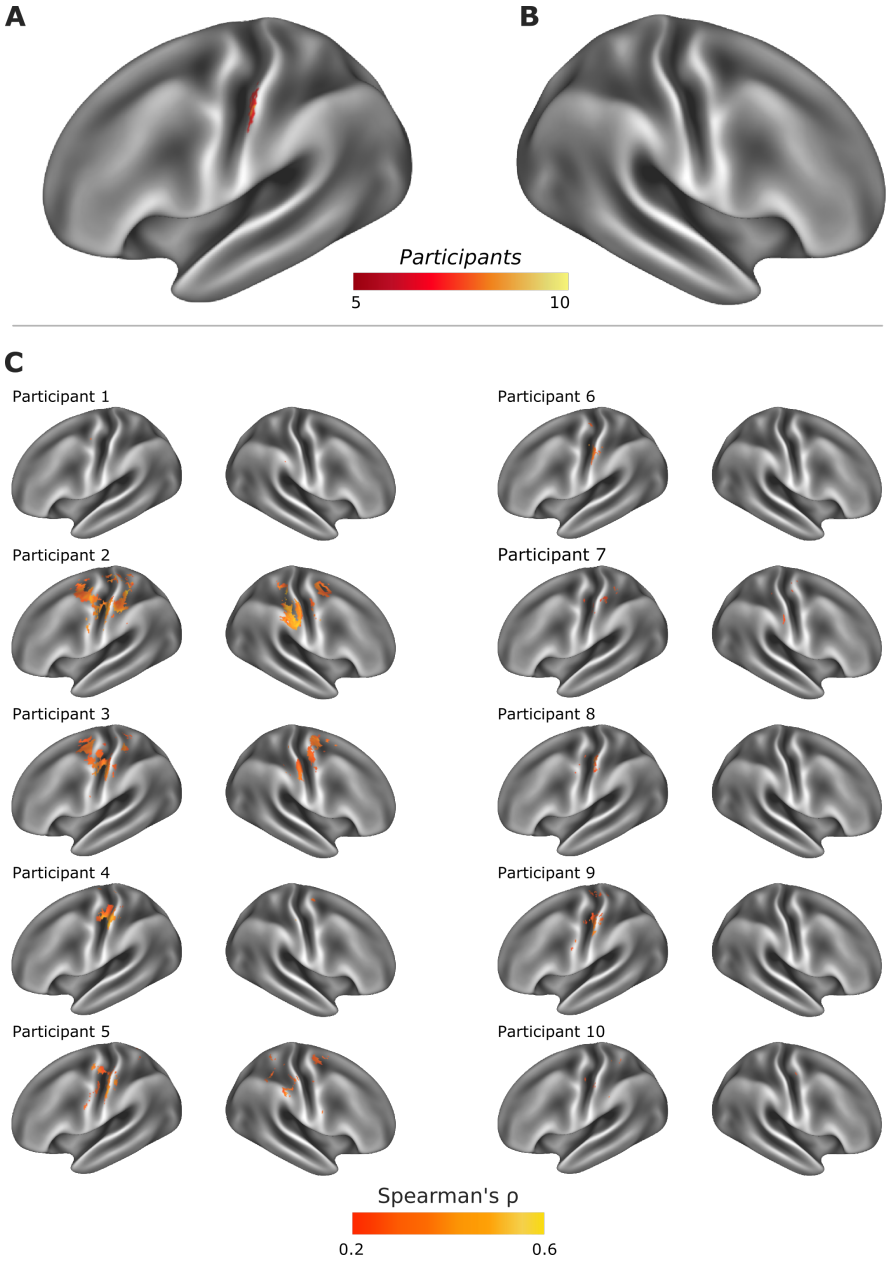

Figure S7: Individual participant cortical searchlight results using an ethological action model of movement encoding. Cortical heatmaps of the left (A) and right (B) hemisphere, show limited but consistent encoding of an action model in the left post-central gyrus, contralateral to movement. Heatmaps were constructed from individually thresholded cortical searchlights for each participant using a single categorical action model (C) (Omnibus threshold, $\alpha = 0.01$, maximum accuracy distribution calculated from peak correlation value across 10,000 searchlight permutations with label-switching.) Supra-threshold range of Spearman's ρ for each participant presented in Table S2.

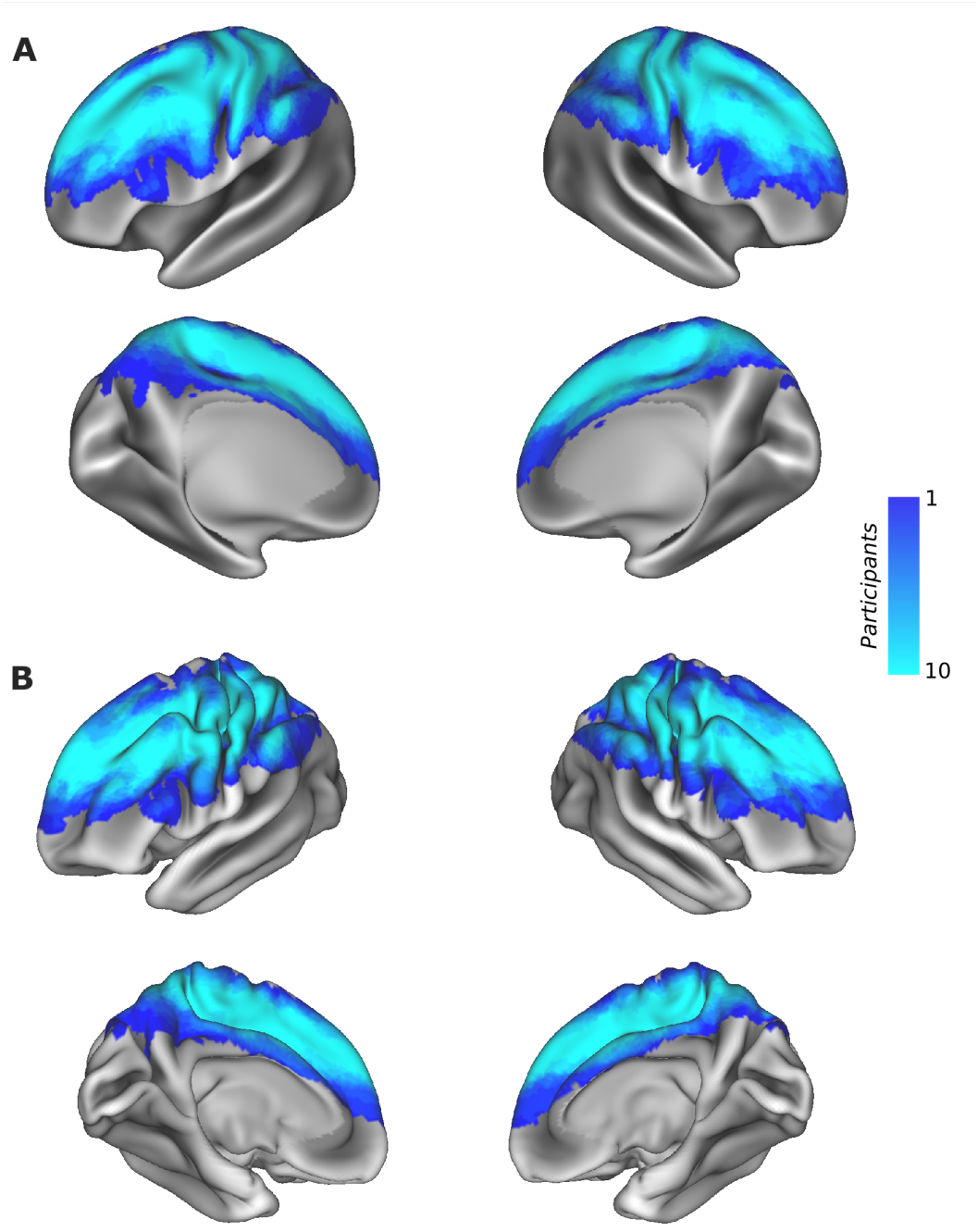

Figure S8: Heatmap surface visualisation of fMRI data coverage across participants on inflated (A) and midthickness (B) surfaces.

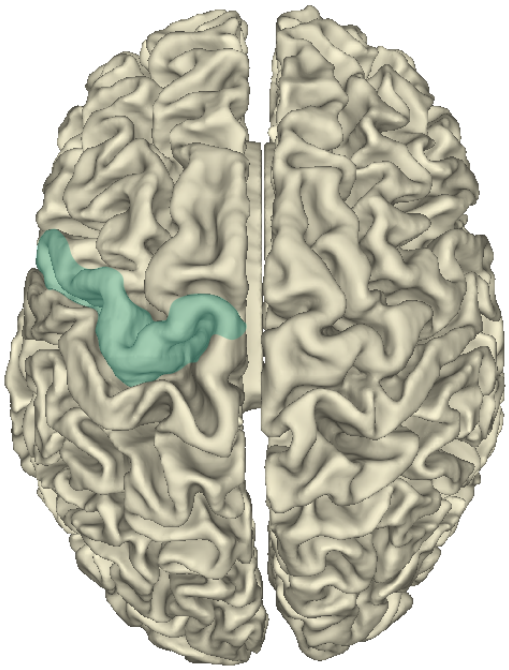

Figure S9: Surface visualisation of the left hemisphere motor region of the AAL atlas used in MEG temporal searchlight analysis: precentral L.

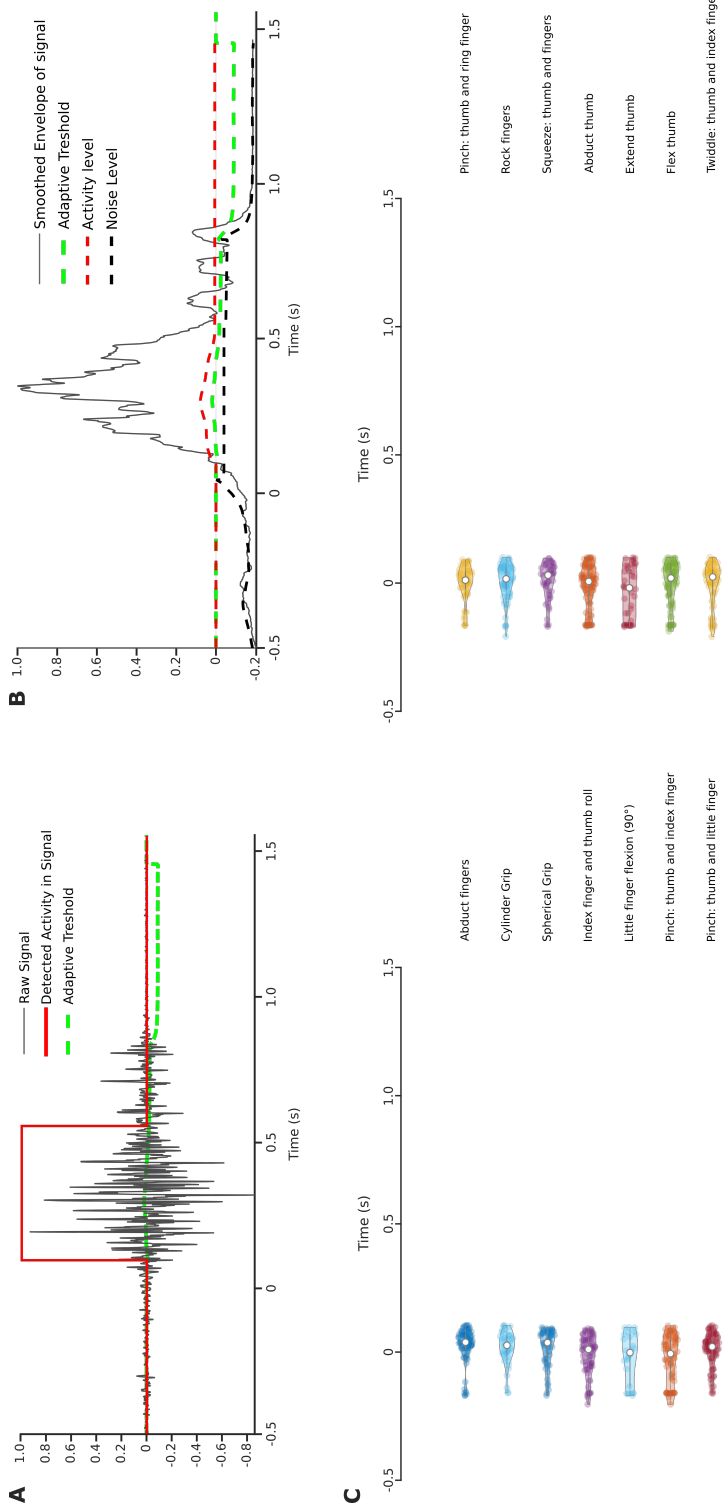

Figure S10: EMG muscle activity onset time. A. Example of EMG onset detection using adaptive threshold. B. Smoothed envelope of signal (Hilbert transform) used for automatic onset detection. C. Violin plots visualising the distribution of EMG onset times for trials from which onset could be detected across all participants. Bars represent interquartile range, white dots represent median values which are plotted in Figure 1. Where available, EMG data were used to validate the data glove derived measures of movement onset used to epoch the MEG data. Time point 0 corresponds to the data-glove movement onset time.

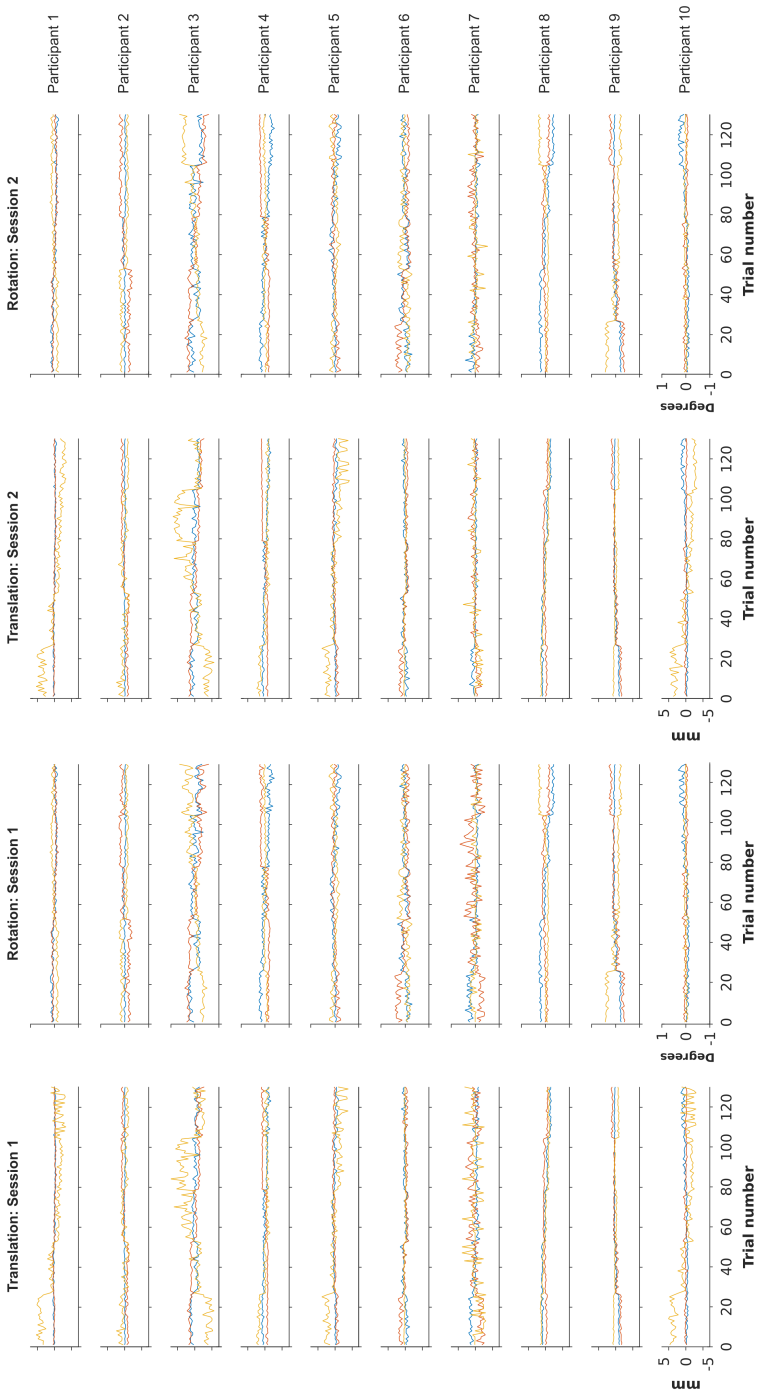

Figure S11: MEG motion timeseries across participants and sessions. Blue: X-axis, orange: Y-axis, yellow: Z-axis

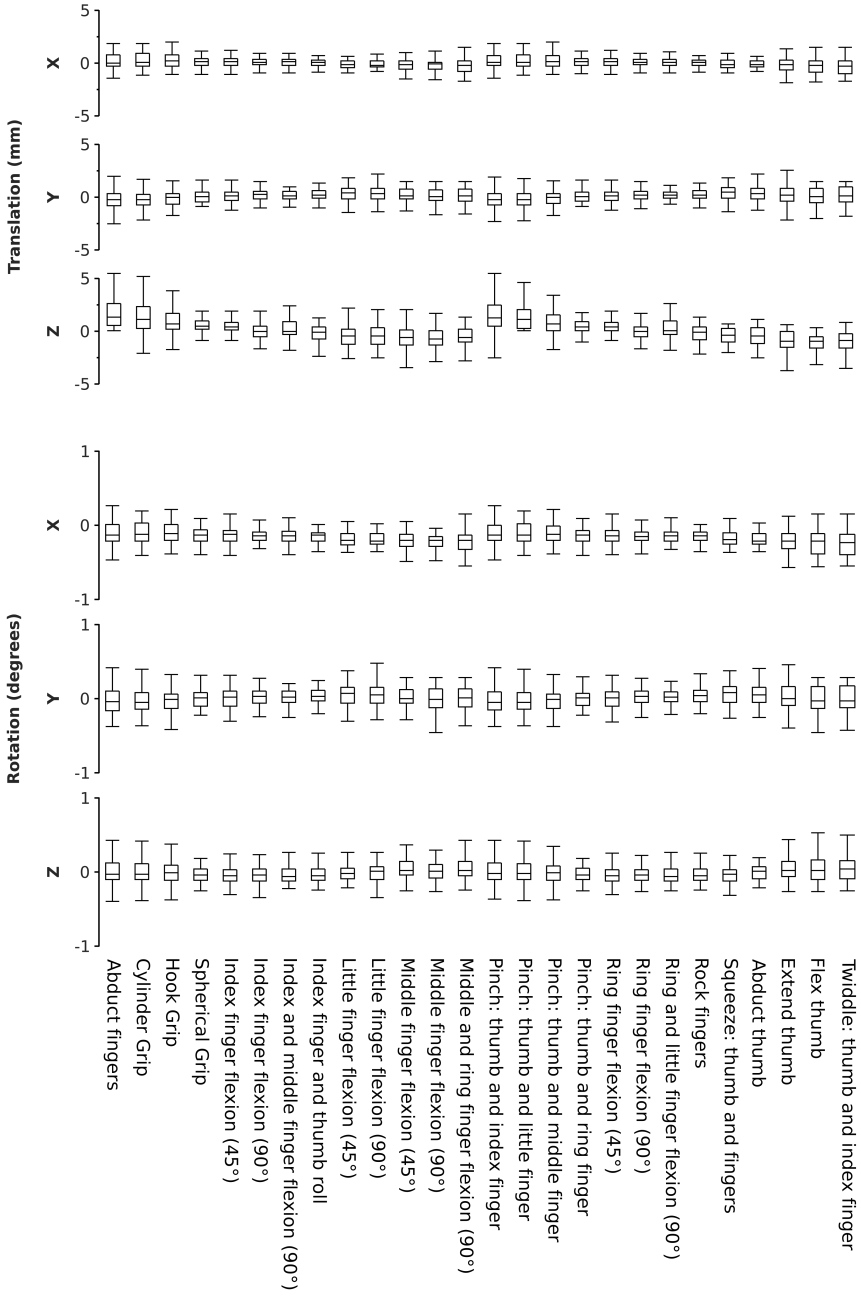

Figure S12: MEG motion comparison across movement conditions.

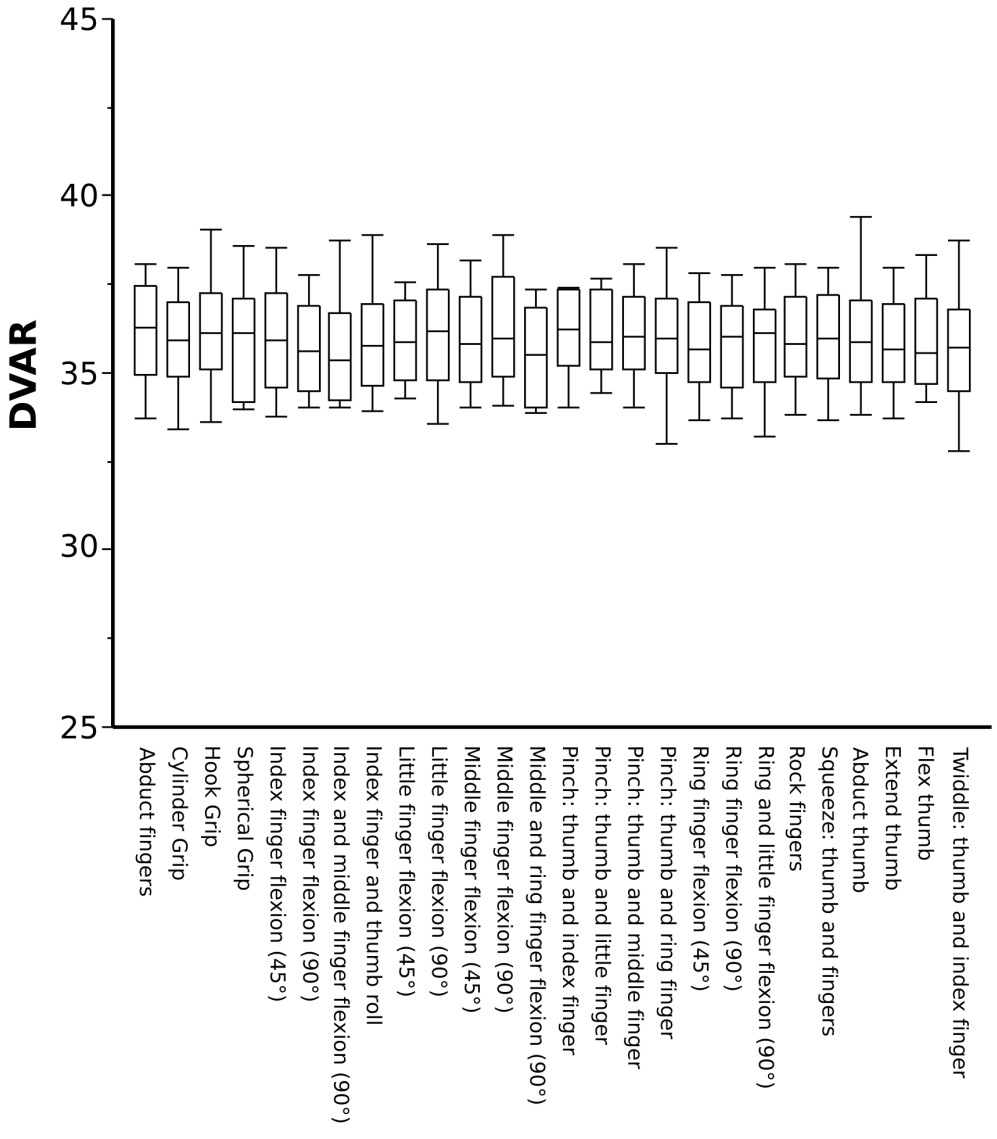

Figure S13: fMRI motion comparison across movement conditions using DVARS presented in arbitrary units[70,78,79].

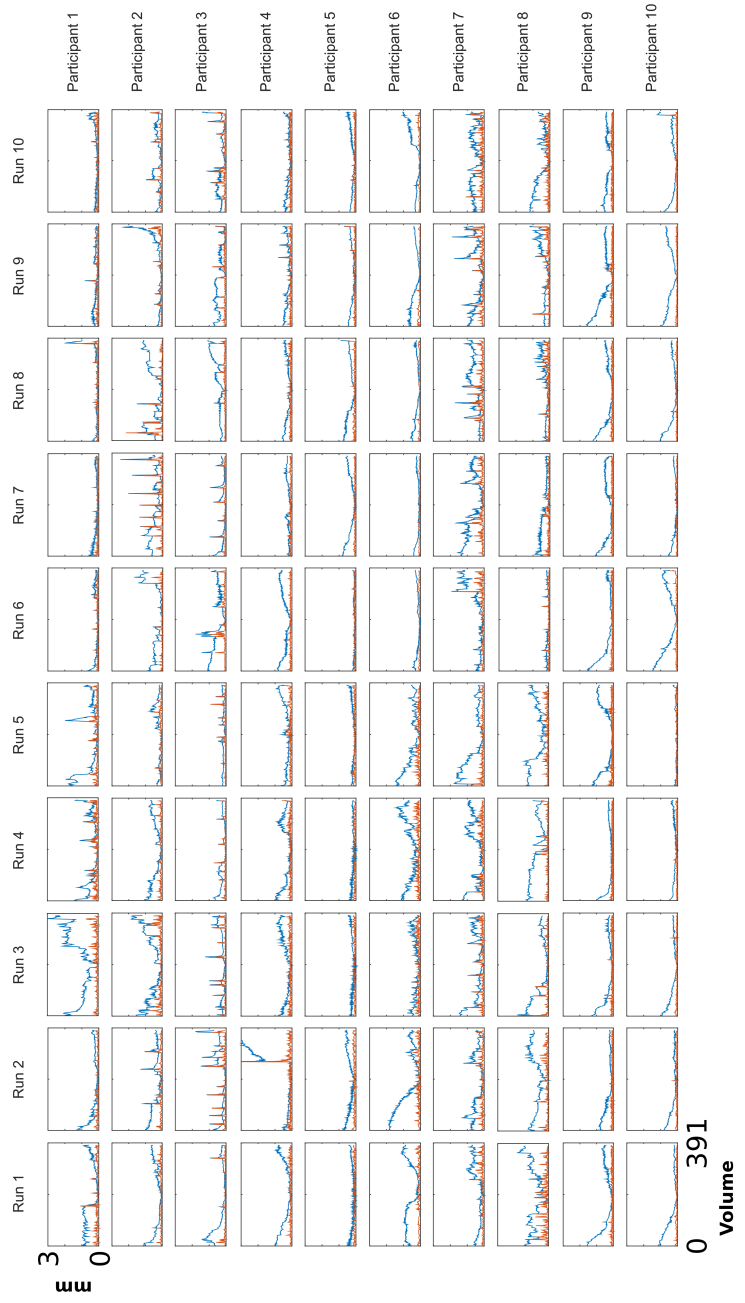

Figure S14: fMRI motion displacement plots. Plots of absolute (blue) and relative (orange) motion calculated using FSL MCFLIRT for each participant and each fMRI task run; motion correction was undertaken prior to ICA denoising.

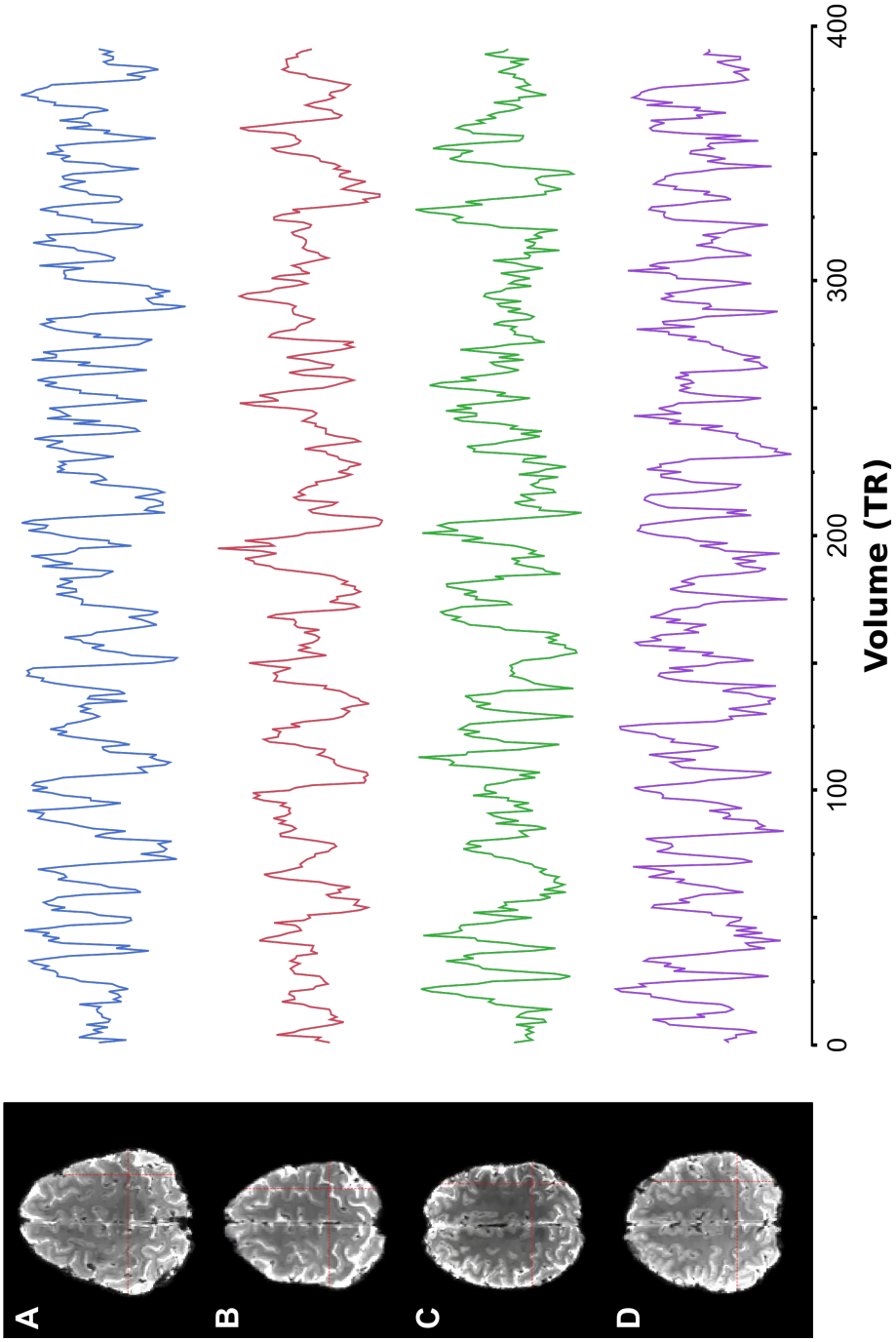

Figure S15: Example fMRI axial slices and single voxel timeseries from 4 participants. fMRI timeseries data extracted from a single voxel (red crosshairs) for four participants. Data presented were subject to high-pass filter (100 seconds). fMRI data were not subject to spatial or temporal smoothing.

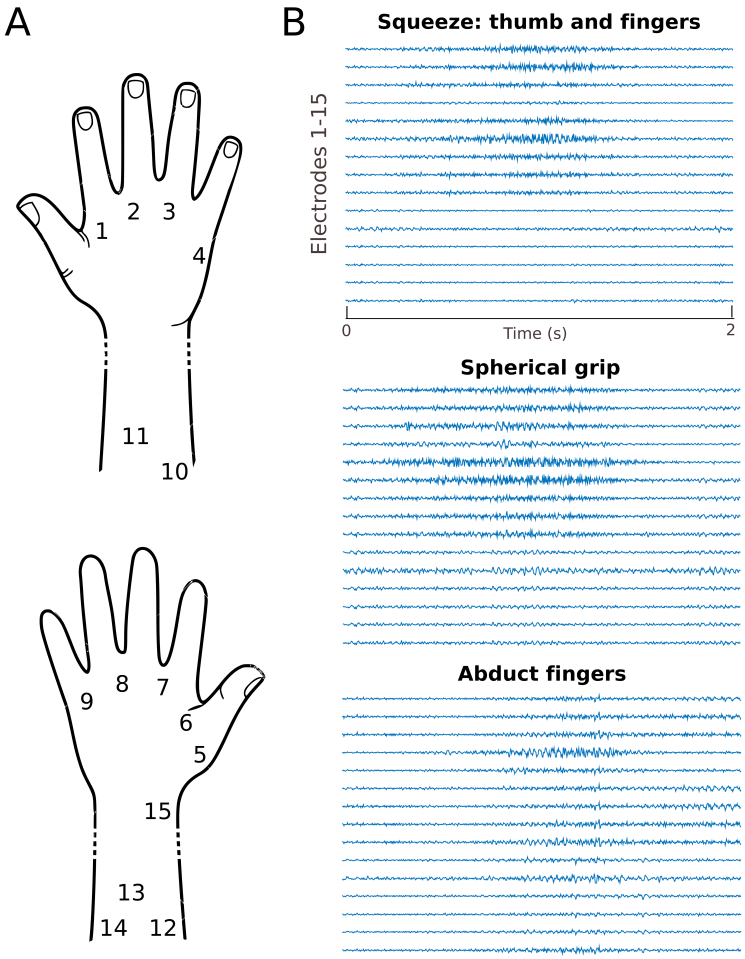

Figure S16: EMG recordings from an independent cohort used to generate a muscle model of hand movement. A) Schematic demonstrating electrode placement for EMG recordings on both the palmar and dorsal surface of the hand and forearm covering these muscles: 1 first dorsal interosseus (FDI), 2-3 dorsal interosseus muscles, 4 abductor digiti minimi, 5 abductor pollicis brevis (APB), 6 adductor pollicis, 7-9 lumbrical muscles, 10 flexor carpi ulnaris, 11 flexor carpi radialis, 12-14 flexor digitorum superficialis and flexor digitorum profundus, 15 flexor pollicis longus. B) Example EMG trace from one participant for three different movements (squeeze, grip sphere and finger abduct) showing electrodes 1-15 across the 2s movement time window.

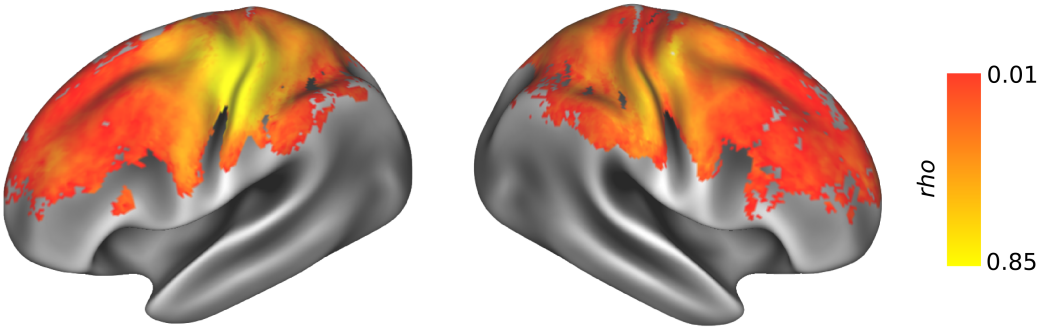

Figure S17: Noise ceiling calculation for spatial searchlight using fMRI data. To assess the spatial consistency in RDMs calculated from fMRI data at each vertex, each participant's RDM was correlated with the average cross-subject RDM; the correlations were then averaged to obtain a vertex-wise upper bound of the noise ceiling.